J Neurophysiol 98: 966–983, 2007.
First published June 20, 2007; doi:10.1152/jn.00421.2006.

Reference Frames for Reach Planning in Macaque Dorsal Premotor Cortex

Aaron P. Batista,[1,2] Gopal Santhanam,[1] Byron M. Yu,[1] Stephen I. Ryu,[1,3] Afsheen Afshar,[1,4] and Krishna V. Shenoy[1,2]

[1]*Departments of Electrical Engineering and* [3]*Neurosurgery,* [2]*Neurosciences Program,* [4]*Medical Scientists Training Program, Stanford University, Stanford, California*

Submitted 21 April 2007; accepted in final form 15 June 2007

Batista AP, Santhanam G, Yu BM, Ryu SI, Afshar A, Shenoy KV. Reference frames for reach planning in macaque dorsal premotor cortex. *J Neurophysiol* 98: 966–983, 2007. First published June 20, 2007; doi:10.1152/jn.00421.2006. When a human or animal reaches out to grasp an object, the brain rapidly computes a pattern of muscular contractions that can acquire the target. This computation involves a reference frame transformation because the target's position is initially available only in a visual reference frame, yet the required control signal is a set of commands to the musculature. One of the core brain areas involved in visually guided reaching is the dorsal aspect of the premotor cortex (PMd). Using chronically implanted electrode arrays in two Rhesus monkeys, we studied the contributions of PMd to the reference frame transformation for reaching. PMd neurons are influenced by the locations of reach targets relative to both the arm and the eyes. Some neurons encode reach goals using limb-centered reference frames, whereas others employ eye-centered reference fames. Some cells encode reach goals in a reference frame best described by the combined position of the eyes and hand. In addition to neurons like these where a reference frame could be identified, PMd also contains cells that are influenced by both the eye- and limb-centered locations of reach goals but for which a distinct reference frame could not be determined. We propose two interpretations for these neurons. First, they may encode reach goals using a reference frame we did not investigate, such as intrinsic reference frames. Second, they may not be adequately characterized by any reference frame.

INTRODUCTION

When we reach out to grasp an object we see, our brain must rapidly determine an appropriate pattern of muscular contractions that will bring the hand to the object. This computation is conceptualized as a reference frame transformation from the initial retinal representation of an object's location to a pattern of muscular contractions. Investigators attempt to determine the reference frame employed by neurons involved in reaching as a prerequisite to understanding how reference frames are constructed, and how neural signals flow between them, to enable reaching.

Reach-related neurons tend to exhibit spatial tuning: they are more active before and during reaches to targets at some locations than others. For an idealized neuron, its reference frame is defined by the part of the body to which the region of selectivity (termed a response field) is rigidly anchored. If that body part moves, the neuron's response field will move in tandem with it; if other body parts move, the response field will not be altered. For example, a hypothetical neuron with an eye-centered reference frame will signal the location of an object relative to the point of visual fixation: as the direction of gaze changes, the neuron's response field moves with it. If other body parts move—the hand, for example—the spatial tuning of such a neuron would not change.

Spatial coding in most cortical neurons is more complex than this idealized case. For example, areas 7a and LIP in the posterior parietal cortex exhibit gain fields: neurons encode visual stimuli in eye-centered reference frames, but responses are scaled by the position of the eyes in the head (Andersen et al. 1985). Some neurons in area LIP (Stricanne et al. 1996) and MST (Bradley et al. 1996) exhibit partial shifts: rather than being rigidly attached to a body part, the region of spatial selectivity of such a neuron moves only partway along with it. Some neurons in parietal area VIP encode visual stimuli using a reference frame that is rigidly attached to the eyes along one dimension yet rigidly attached to the head along a perpendicular dimension (Duhamel et al. 1997). In parietal area 5 (Buneo et al. 2002) and in premotor cortex (Pesaran et al. 2006), neurons have been identified that encode reach goals using a reference frame defined by the combined position of two body parts—the eyes and hand. Other deviations from the strict definition of a reference frame are conceivable; it is even conceptually possible that a neuron might exhibit no reference frame—the location to which such a cell is most sensitive might be influenced by the position of one or more body parts, while bearing no consistent spatial relationship to any one or combination of them.

The reference frame transformation for reaching is thought to take place within a network of cortical areas between the parietal and frontal lobes (reviewed in Boussaoud and Bremmer 1999; Caminiti et al. 1996; Kalaska et al. 1997). An important node in this network is the dorsal aspect of the premotor cortex (PMd). Numerous studies indicate that PMd is involved in the planning and performance of visually guided reaches. Individual neurons are active during the delay period preceding an instructed movement (Weinrich and Wise 1982). Neurons are tuned for the direction (Caminiti et al. 1991; Fu et al. 1993) and distance (Messier and Kalaska 2000) of reaches. Inactivation of PMd causes deficits in reaching, in particular for complex stimulus-response associations (Kurata and Hoffman 1994; Moll and Kuypers 1977). Microstimulation in PMd delays reaches (Churchland and Shenoy 2007). Parameters related to the details of the movement, for example, the orientation of the arm (Scott and Kalaska 1997) and the speed of the reach (Churchland et al. 2006b), are encoded in PMd.

Address for reprint requests and other correspondence: K. V. Shenoy, 319 CISX, 330 Serra Mall, Paul G. Allen Center for Integrated Systems, Department of Electrical Engineering and Neurosciences Program, Stanford University, Stanford, CA 94305-4075 (E-mail: shenoy@stanford.edu).

The costs of publication of this article were defrayed in part by the payment of page charges. The article must therefore be hereby marked "*advertisement*" in accordance with 18 U.S.C. Section 1734 solely to indicate this fact.

Neural activity during the delay period preceding a reach is predictive of the movement's reaction time (Churchland et al. 2006c; Riehle and Requin 1993) and peak speed (Churchland et al. 2006a).

PMd receives anatomical input from the posterior parietal cortex, including some of the areas that comprise the parietal reach region (Caminiti et al. 1996; Matelli et al. 1998; Tanne-Gariepy et al. 2002). The parietal reach region is known to encode reach goals in eye-centered coordinates (Batista et al. 1999; Buneo et al. 2002; Cisek and Kalaska 2002; Pesaran et al. 2006). In turn, PMd projects to the spinal cord (Dum and Strick 1991; Galea and Darian-Smith 1994) and to the primary motor cortex (Matsumura and Kubota 1979). Because PMd receives at least some of its information about reach targets in eye-centered coordinates and because it sends outputs almost directly to neurons that control the arm muscles, it is important to establish the reference frame(s) in which PMd encodes reach goals.

Evidence for a variety of reference frames in PMd has been reported. In an early investigation of the reference frames used by PMd, Caminiti et al. (1991) reported that PMd neurons encode reach goals relative to the shoulder. Since then, studies indicate that eye position modulates PMd neurons (Boussaoud et al. 1998), although more recent evidence supports only a modest effect eye position (Cisek and Kalaska 2002). Recently, the presence of a reference frame that encodes reach targets relative to the combined position of the hand and eyes was reported (Pesaran et al. 2006). Outside PMd, in other cortical areas related to reaching, other reference frames have been observed. Coding of reach targets relative to the hand has been reported in primary motor cortex (Georgopoulos et al. 1986). Coding of visual stimuli relative to tactile receptive fields on the arm has been reported in the ventral aspect of the premotor cortex (Graziano and Gross 1998; Graziano et al. 1994, 1997b). Each of the aforementioned reference frames is *extrinsic*; that is, visual stimuli are encoded as locations in external space, relative to a particular body part. There is also evidence that regions involved in motor control use *intrinsic* reference frames; for example, some neurons encode the joint rotations (Scott et al. 1997) or muscular contractions (Kakei et al. 1999; Kalaska et al. 1989) required to perform movements.

We developed an experimental paradigm that could examine PMd responses in several different extrinsic reference frames. Reach goals were found to be encoded in a variety of reference frames by different neurons within PMd, including limb-centered, eye-centered, and reference frames defined by the relative position of the hand and eyes. We also observed many neurons that could not be characterized by any of the extrinsic reference frames we tested. Two possibilities are proposed for the spatial tuning of these neurons. First, they might encode reaches using some reference frame we did not test, including intrinsic reference frames. Second, these neurons may not employ any reference frame. That is, because the response field shape is affected by both the eye- and limb-centered position of the targets but moves in tandem with neither of them (separately or in combination), these cells may not be usefully characterized by any reference frame.

Brief reports of this work have appeared (Batista et al. 2004, 2005).

METHODS

Animals

Two adult male Rhesus macaques (*Macaca mulatta*) were employed in this study. *Monkey G* weighed 8 kg, and *monkey H* weighed 15 kg. All protocols were approved by Stanford University's Institutional Animal Care and Use Committee. Their training histories were highly similar as both animals had participated in the same experiments prior to this study (Santhanam et al. 2006; Yu et al. 2007). Experiments were performed 4–5 mo after array implantation for *monkey G* and 7–9 mo after implantation for *monkey H.*

Surgical preparation

Recordings were performed with a chronically implanted 10 × 10 array of electrodes (Cyberkinetics Neurotechnology Systems, Foxborough, MA) surgically implanted in PMd (Fig. 1) under aseptic conditions. Electrode spacing was 0.4 mm. Electrodes were 1.0 mm long, and array impaction was designed to target layer 5. The array was positioned to coincide with the region of PMd that projects to the spinal cord, and to the primary motor cortex (Dum and Strick 1991, 2005; He et al. 1993). Experimental sessions began no sooner than 1 wk after surgery.

Functional confirmation of array placement in PMd

In *monkey G,* electrode placement in PMd was verified by microstimulation ~1 yr after these experiments were conducted. (At that time, neurons were still observed on several channels, indicating that the array was still embedded in cortex.) Movements that included rotations at any or all of the shoulder, elbow, and wrist joints were evoked with thresholds between 40 and 240 μA (200–333 Hz, 20 pulses) by microstimulation at nearly all electrodes.

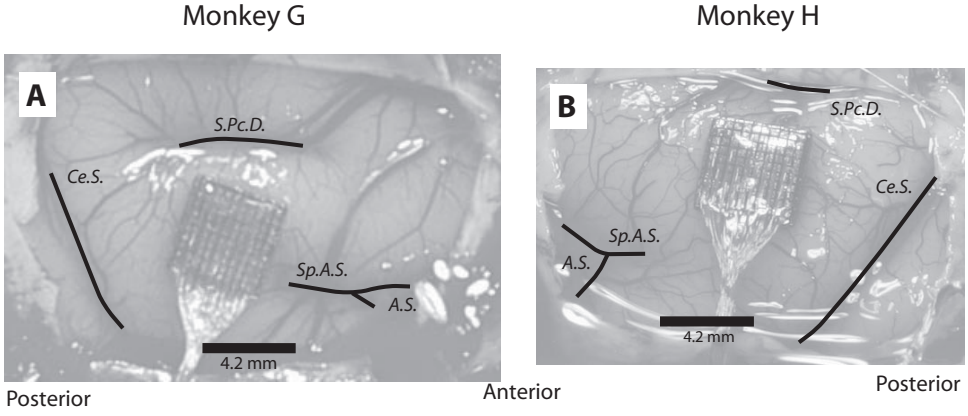

FIG. 1. Placement of electrode arrays. Intraoperative photographs of arrays implanted in dorsal aspect of the premotor cortex (PMd) with sulci indicated. Sulcal landmarks were drawn by hand on magnified, full-color, full-contrast versions of these photographs, then pasted in register on these images. Ce.S., central sulcus; S. Pc. D, superior precentral dimple; Sp. A. S., spur of the arcuate sulcus; A. S., arcuate sulcus.

Apparatus for behavioral monitoring

Monkeys sat in a primate chair (Crist Instrument, Hagerstown, MD) that allowed nearly unrestricted movement of the arm contralateral to the electrode array (left arm for *monkey G,* right arm for *monkey H*) but comfortably restrained the ipsilateral arm. The head was braced via a surgically implanted head holder. Experimental control and data collection were under computer control with TEMPO (Reflective Computing, St. Louis, MO). Animals faced a large vertically oriented flat screen (90 cm horizontal × 60 cm vertical, 27 cm from the eyes, centered vertically at approximately shoulder height, and horizontally on the midpoint of the eyes) onto which visual stimuli were rear-projected using a CRT projector (Barco 1208s, Logan, UT). The animal's hand position was monitored in three dimensions using the Polaris system (NDI, Waterloo, Ontario, Canada). A small reflective marker was taped to the distal digit of the third finger, and its position (to nominal submillimeter resolution) was monitored in the infrared at 60 sample/s. Eye position was monitored (~1° resolution, 240 sample/s) using an infrared camera that tracked the pupil (Iscan, Burlington, MA). Monkeys were rewarded for correct task performance with water or juice.

To measure the exact timing of the appearance of visual stimuli, we used a custom-built photodetector. Whenever a new visual stimulus appeared, in the same video frame, a small spot was presented out of the monkey's view. That flash was detected by the photodetector, and the time of its occurrence was stored at 1-ms resolution. In off-line data analysis, these photodetector times were used for aligning the data.

During experiments, the animal worked alone in a sound-attenuating chamber. The room was completely dark except for the visual stimuli. Use of a CRT projector ensured there was no background illumination.

Behavioral task

Monkeys were trained to perform a reference frame task (Fig. 2*A*). Each trial began with the appearance of a yellow square (20 mm on a side), termed the touch point (TP). After the monkey touched the TP (within a tolerance window extending 7.5 mm beyond the edges of the touch point on each sides), the fixation point (FP, a purple cross 8 mm across) appeared. Four hundred milliseconds after the monkey directed his gaze at the FP, the reach target (a second yellow square 10 mm on a side) appeared. The TP and FP remained illuminated, requiring the monkey to maintain his hand and eye posture, for an additional 750- or 950-ms delay period. (For *monkey G,* a brief 250 ms delay period was presented on 20% of the trials, as a "catch" trial, to encourage him to plan throughout the delay period. Data from these catch trials were not analyzed. For *monkey H,* catch trials were used during training but not during experiments.) At the end of the delay period, the FP and TP were extinguished, and the peripheral target was enlarged to 20 mm on a side as the "go" signal. The monkey then reached to the target. Ninety-eight percent of reaches were initiated within 400 ms; those that took longer were excluded from analysis because the monkey may have not planned the reach until after the go cue (Churchland et al. 2006c describes the relationship between PMd delay-period activity and reaction time.) Eye position was unconstrained after the go signal, so the monkey was free to look at the target as he reached toward it. Once the target was held for 300 ms, the monkey was rewarded. An audible tone accompanied the delivery of the juice reward.

We manipulated the location of the touch point, fixation point, and target on each trial (Fig. 2*B*). The task was designed to independently assess the effects on neural activity of target position relative to the eyes and the hand (Batista et al. 1999; Buneo et al. 2002; Cohen and Andersen 2000). Four different *start configurations* (that is, initial hand and eye positions) were used. The four start configurations

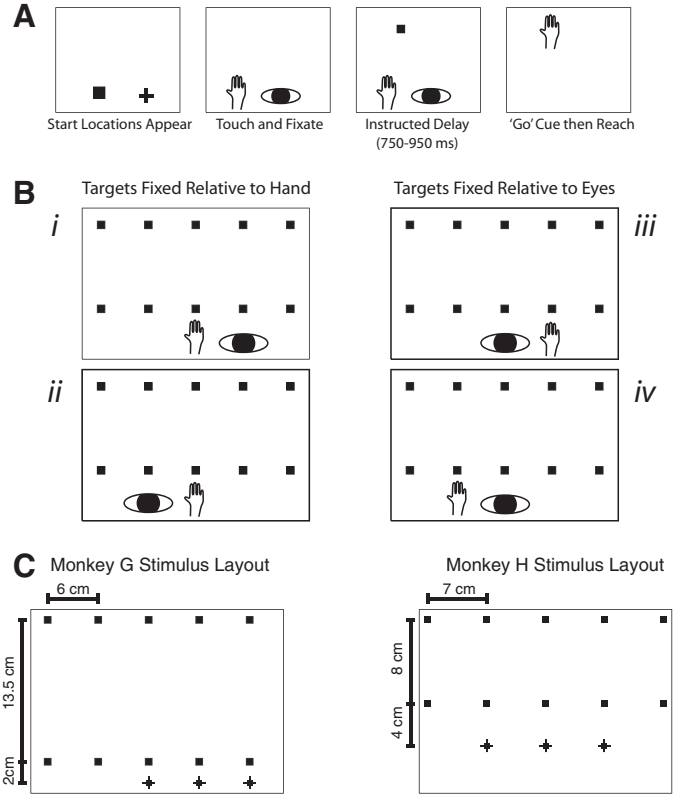

FIG. 2. Reference frame task. *A*: timeline. From left to right, touch point and fixation point appear and are acquired by the monkey. Reach target appears at a peripheral location. The monkey withholds his movement through a delay period. When the touch and fixation points are extinguished, the monkey reaches to the target to obtain his reward. *B*: geometry. Each panel shows 1 of the 4 possible start configurations (i–iv) with 10 possible targets. *C*: typical stimulus layouts for each animal. In the figure, the 4 start configurations are superimposed, hence overlapping + and ■ in the *bottom row.*

grouped into two pairs: In one pair (start configurations iii and iv, Fig. 2*B, right*), the eye position is the same, whereas the initial hand position is different. Thus a given target is at the same location in eye-centered coordinates between the two conditions but is at different locations relative to the hand and arm. In the other pair of start configurations (start configurations i and ii, Fig. 2*B, left*), the initial hand position is the same but the fixation point differs. This manipulation altered the locations of the targets in eye-centered coordinates while maintaining them in limb-centered coordinates. For each of the four start configurations, reaches were instructed to targets at the same locations (relative to the screen). All targets were presented above the initial eye and hand position; during pilot experiments, when the targets were presented below the level of the eyes and hand, some were obscured by the monkey's arm, and he minutely adjusted his arm posture to observe them. These minute movements may have been sufficient to drive PMd activity, so we selected the task geometry to eliminate the need for them.

Target locations and start positions were chosen prior to recording to span the limits of the range over which the monkey could consistently reach. Thus slightly different geometries were used for the two animals. The workspaces used for *monkey G* were either 10 targets arrayed in two rows spanning 24 × 13.5 cm (51 × 29° of visual angle), positioned 2 cm (4°) above the row of start configurations (Fig. 2*C*, *left*) or 28 targets arrayed in four rows spanning 27 × 13.5 (57 × 29°). For *monkey H,* the workspace was ten targets arranged in two rows spanning 28 × 8 cm (59 × 17°) and 4 cm (8°) above the row of start configurations (Fig. 2*C*, *right*). A second difference in the

stimulus layout between the two monkeys is evident in Fig. 2*C*. For *monkey G,* we presented the targets with a slight contralateral bias. Because the response fields recorded in this monkey (the first studied in this experiment) did not show a strong laterality (data not shown), we used a symmetric target placement for *monkey H.*

All task conditions (all combinations of the 4 start configurations and 10 or 28 target locations) were randomly interleaved.

Eye-position control

Trials in which the eye position exceeded a tolerance window around the FP of ±10 mm (2°) horizontally and ±15 mm (3°) vertically were excluded during analysis. Trials in which eye position exceeded a somewhat larger window [60 mm (±6°) for *monkey G* and 40 mm (±4°) for *monkey H*] were aborted during the experiment.

Hand position

Hand position traces were digitally low-pass filtered at 25 Hz. To determine hand velocity, we differentiated the hand-position traces, and again filtered at 25 Hz. Reaction time was determined by detecting the time when the hand velocity first exceeded 20% of the peak hand velocity. Movement duration was measured from then until the earliest time when hand velocity fell <20% of the peak velocity.

Neural recordings

As the electrodes could not be moved, we observed a range of neural signals across the array from well-isolated to multiunit. For *monkey G,* we manually discriminated action potential waveforms at the start of each session, using two time-amplitude window discriminators on each channel (Cyberkinetics Neurotechnology Systems). Discriminations were made during an initial ~20-min block while the monkey performed the task. Well-isolated single units were discriminated with zero, one, or two units detected on each electrode. Multiunit isolations were also noted and recorded, although those data were not analyzed. Once the discriminator windows were set, data storage began, and the windows were no longer adjusted. Array recordings are quite stable within recording sessions: we did not observe drift in the isolations throughout the day.

For *monkey H*'s recording sessions, we used an automatic algorithm for waveform discrimination. The procedure is summarized here (see Sahani 1999; Santhanam et al. 2004 for fuller descriptions). An automated spike-sorting system monitored signals from each electrode during a 2-min period at the start of each recording session while the monkey performed the task. Data were high-pass filtered, and a threshold was established at three times the root mean square of the signal amplitude of each channel. The portions of the signal from each electrode that did not exceed the threshold were used to characterize the noise on that channel. Then during experiments, a snippet of the signal was saved at the time of each threshold-crossing, from 0.3 ms before the threshold-crossing until 1.3 ms after. These snippets were stored at 30 ksample/s. After the experiment, the snippets were processed: first, snippets were noise-whitened, using the noise estimate made at the start of the experiment. Noise-whitening accounts for the covariance in the background process so that the clusters are close to Gaussian and circularly symmetric. Snippets were trough-aligned, then transformed into a four-dimensional space using a modified principal components analysis (Fig. 3*A*). Automatic processes estimated the number and locations of the optimal number of clusters in the principal-components space. This process initially overestimated the number of clusters; then one or more clusters were grouped together to correspond to one putative neuron with a distribution of waveforms (Fig. 3*B*). There were two special clusters, in addition to those arising from neural events: one for the background noise and another for outliers. The results of the algorithm were then certified by experienced neurophysiologists. We visually inspected

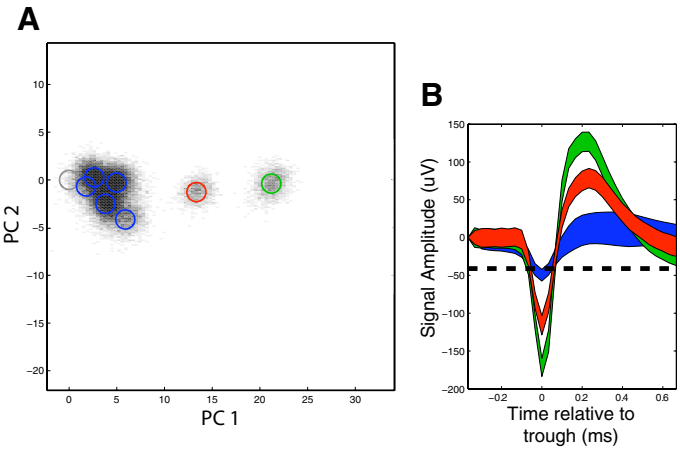

FIG. 3. Automated spike sorting for 1 electrode. *A*: principal components analysis of neural waveforms. The axes are the weights of the 1st 2 principal components. Each point indicates 1 threshold-crossing event. Red, green, and blue circles indicate the clusters determined automatically. *B*: waveform plots. Each trace is an envelope containing 80% of the waveforms that were assigned to each cluster. The red and green clusters were selected for inclusion in the analyses, and the blue cluster was discarded.

each cluster in principal-components space and the distributions of waveforms assigned to it. Only units with isolations that were on par with isolation qualities attained in traditional single-electrode studies were analyzed. (Kelly et al. 2007 reports that array recordings and recordings with traditional moveable electrodes are comparable in quality.)

In recordings performed with chronic multielectrode arrays, it is possible to record stable, well-isolated neurons that have extremely low firing rates in the task. We eliminated from analysis any neurons with a firing rate of three spikes per second or less during the delay period in all task conditions.

Data sets

Data collected during all days when the reference frame task was performed are presented here. Two datasets were collected 6 days apart in *monkey G,* and three datasets were collected in *monkey H* (first and last datasets 6 wk apart.) *Monkeys G* and *H* successfully performed 77 and 79% of trials per day on average, respectively. Over all five datasets, an average of 5–18 successful repetitions of each task condition were included in the analysis. The principal findings did not differ when days were analyzed separately.

Across all five recording sessions, 362 well-isolated units were recorded. Each day, well-isolated neurons were found on 46–56 electrodes. On electrodes where neurons were found, there were averages of 1.2 and 1.5 well-isolated neurons per electrode for *monkeys G* and *H,* respectively. Of these, 212 had a firing rate in excess of three spikes per second during the delay period for at least one task condition. Only these cells were analyzed. Seventy-four of these neurons came from *monkey G* (36 and 38 per day), and 138 were from *monkey H* (42–49 per day). We did not attempt to track individual neurons over days, nor did we attempt to verify that neurons recorded on different days were distinct because systems that can allow continuous long-term tracking of cell identities are only now becoming available (Jackson et al. 2006; Santhanam et al. 2007). Thus additional recording days with each animal serve both to expand the cell count and also to verify that the properties we observed were stable over time.

Data analysis

Data analysis was performed using Matlab (The Mathworks, Natick, MA). All analyses used the firing rate during the 500-ms

epoch extending from 250 ms after the appearance of the reach target until the time of the earliest go cue. We excluded the initial 250-ms period to allow enough time for information about target location to arrive in PMd, and for any visual transients to subside (Churchland et al. 2006c; Santhanam et al. 2006). This 500-ms epoch is termed the delay epoch.

The firing rate of a neuron during the delay epoch as a function of target location will be termed a *response profile*. Thus for each neuron, four response profiles were measured, corresponding to the four start configurations shown in Fig. 2*B*.

Three separate measurements of the reference frames used in PMd were performed and are described in the following text. The first method directly compares the impact of changing the locations of the targets relative to the eyes to the impact of changing the locations of the targets relative to the limb. The second method characterizes the reference frame for each neuron by determining the horizontal shift that brings each pair of response profiles into their best alignment. The third method measures how discriminable are different start configurations and target locations across the population of simultaneously recorded neurons.

Data analysis 1: sensitivity

We measured how sensitive each neuron was to the location of the reach target relative to either the eyes or the arm and compared those two sensitivities. For example, a neuron that employed an eye-centered reference frame would be sensitive to the location of the targets relative to the eyes and insensitive to the location of the targets relative to the arm. We quantified the similarity between the response profiles within each pair of start configurations (i.e., between configurations i and ii and between configurations iii and iv, shown in Fig. 2*B*) by computing the normalized Euclidean distance between them

$$dist = \frac{\sqrt{\sum_{i=1}^{T}(n_i - m_i)^2}}{\sqrt{T}} \quad (1)$$

where n and m are normalized response profiles. (Response profiles were normalized between 0 and 1 by first subtracting the smallest firing rate observed in the two response profiles from all values, then scaling all firing rates by the reciprocal of the largest firing rate.) T is the number of targets. The denominator ensures that the distance metric is bounded between 0 (meaning the response profiles were identical) and 1 (meaning the normalized response profiles were maximally different).

Measurement error in the distance metric was estimated. For each neuron that was tuned in the task (single-factor ANOVA, factor: target location, $P < 0.05$, Bonferroni corrected for multiple comparisons across the 4 start configurations), a synthetic response profile was computed by randomly resampling N trials (with replacement) from the N repetitions of reaches to each target, then averaging. For each start configuration, this was done twice, and the distance between these synthetic response profiles was computed using *Eq. 1*. This procedure was repeated 1,000 times, and the average value was computed. Then the distance values for each pair of start configurations (columns in Fig. 2*B*) were averaged. This procedure yielded two values for each neuron, which were plotted against one another in Fig. 6 (gray squares). Deviations from (0,0) constitute measurement error due to variability in neural firing rates.

Confidence intervals on the distance metrics were estimated using a bootstrap test. Synthetic response profiles were created by drawing N firing rates (with replacement) from the N repetitions of experimentally determined firing rates. The Euclidean distance was recomputed using these N firing rates. (Note that data were not shuffled across target locations or start configurations.) Ten thousand iterations were performed, and confidence intervals were estimated as the range that delimited 95% of the computed distances. These confidence intervals indicate the range within which distance metric would have fallen 95% of the time, assuming that we collected enough trials in the experiment to reflect the true distribution of firing rates.

We also tested whether neurons employed a reference frame defined by the combined position of the eyes and the hand (Buneo et al. 2002; Pesaran et al. 2006). We could test the alignment of each neuron in a combined eye+hand reference frame by pairing the two response profiles collected while the eye and the hand were in a fixed geometry relative to one another (eyes left of hand or eyes right of hand) and shifting them horizontally by one column of targets, so that the targets are aligned relative to the hand and eyes between the two configurations, then computing the Euclidean distance between the realigned response profiles. For example, start configuration i (pictured in Fig. 2*B, top left*) and start configuration iv (Fig. 2*B, bottom right*) can be paired in this way as can start configurations ii and iii. Note that for each neuron, two such shifts are possible: eyes positioned to the left of the hand and eyes to the right of the hand. We retained the smaller (i.e., the better-aligned) of the two computed distances. These shifted, eye+hand-aligned distance values were compared with the smaller of the (unshifted) eye-aligned or hand-aligned distance values for each neuron. In this way, each neuron's best alignment in either eye- or limb-centered coordinates was compared with its best alignment in a combined eye+hand reference frame to determine if the latter reference frame offered a better alignment between the response profiles.

Also the sensitivity analysis would allow us to identify neurons that might use head-centered reference frames (or, indistinguishably here, body- or world-centered). Such cells would be insensitive to both the eye-centered and the limb-centered locations of reach targets; that is, both of their distance values would be low, and statistically indistinguishable both from each other and from zero. Using the estimate of measurement noise for the population, we determined a border that encompassed 95% of the noise values (gray squares in Fig. 6). This border was defined by the line $y + x = 0.48$, where x is the distance between the hand-aligned response profiles, and y is the distance between the eye-aligned response profiles. Candidate head-centered neurons lie inside this border (i.e., $y + x < 0.48$), meaning their sensitivity to eye and hand position were not statistically distinguishable from zero.

Data analysis 2: best shift

We measured the optimal shift between each pair of response profiles, and the gain at that shift. First, the optimal shift was determined by shifting one response profile in each pair (eye-aligned and hand-aligned) horizontally by zero, one, or two target columns, and computing the correlation coefficient between the two response profiles at each shift

$$shift = \arg\min_{x}\left(\frac{\sum_{i=1}^{6}(a_i - \bar{a})(b_i^x - \overline{b_i^x})}{\sqrt{\sum_{i=1}^{6}(a_i - \bar{a})^2}\ \sqrt{\sum_{i=1}^{6}(b_i^x - \overline{b^x})^2}}\right) \quad (2)$$

where a is the unshifted response profile, b^x is the shifted response profile. $X \in \{0,1,2\}$ parameterizes the number of target columns by which the response profile b is shifted. The response profiles are restricted to six target locations that overlap for that shift.

Correlation is insensitive to scale differences between the two vectors. Once the optimal shift was determined, the gain between the two response profiles at that shift was computed as

$$gain = \frac{\sum_{i=1}^{6} \frac{a_i}{b_i + \varepsilon}}{6} \quad (3)$$

where ε is a small constant.

Data analysis 3: decoding

To explore reference frames across a population of simultaneously recorded neurons, we employed a decoding analysis. This analysis answers the question: given the distribution of activity across the neural population for one trial, can we estimate which start configuration and target location were instructed for that trial? Each trial is set aside in turn, and a model of population neural activity as a function of start configuration and target location is trained using the remaining trials. The model is tested using the trial that was set aside to determine how well the neural population can discriminate different target locations and start configurations. (This approach is known as leave-one-out cross-validation.) The procedure is summarized here; details can be found in Batista et al. (2007).

Neural activity as a function of task geometry (that is, start configuration and target location) was assumed to follow a Poisson distribution. During training, for each neuron x_n in the population of N neurons recorded simultaneously, the average spike count across all M task geometries (here, $M = 10$ targets * 4 start configurations) is computed. During testing, the task geometry m that maximizes the likelihood of the observed spike counts for the test trial $\bar{x}$ is estimated. The performance of the decoder is quantified by comparing the actual to the decoded task geometry for every trial.

This analysis was performed using one day's data for each animal; the day with the greatest number of successful trials was used.

Regression of neural activity against behavior

Slight differences between the parameters of the reaches performed in the different start configurations were observed. We explored whether the small differences in the endpoint of the reach between start configurations i and ii could account for the observed differences in firing rates. (At least some of the remaining variability is due to the differences in the retinal locations of the reach goals between the two start configurations.)

We analyzed start configurations i and ii because the instructed reach vectors are the same, whereas the fixation points differ. We calculated the difference in firing rate that we would expect due to the difference in endpoint along the horizontal axis (assuming that the fixation position had no effect) and compared that to the actual difference in firing rate for the two different fixation positions. We first determined the target location for which the largest separation in mean reach endpoint for the two different fixation conditions was observed. We then performed, for each neuron, a linear regression between firing rate and the instructed endpoint for the row of targets that contained the target for which the largest separation in endpoints was observed. From the regression, we estimated the difference in firing rate that would be expected due to the difference in mean endpoint in the two conditions. We compared this value to the actual difference in firing rate observed for reaches to that location when the initial fixation configuration was different. The ratio of these two firing rate indicates the fraction of the difference in firing rate between the two fixation conditions that can be accounted for by the difference in mean reach endpoint under the two conditions.

RESULTS

Neurons recorded (212) in two animals were included in analyses (see METHODS). One hundred fifty four of them (73%) were tuned for target location in at least one start configuration (single-factor ANOVA, $P < 0.05$, Bonferroni corrected for multiple comparisons). One-hundred-forty-three neurons (67%) were modulated by changing the initial position of the hand (main or interaction effects in a 2-factor ANOVA, with factors: target location and hand position). One-hundred-twenty-two (58%) neurons were modulated by changing the eye position (2-factor ANOVA, 2nd factor: eye position). Thirty-one neurons (15%) were modulated by neither eye or hand position.

PMd neurons employing hand- and eye-centered reference frames

Figure 4*A* illustrates responses during the task for one PMd neuron. Each of the 40 subplots is a peristimulus time histogram (PSTH) depicting average neural activity as a function of time for one task condition. The four start configurations are grouped separately, and within each grouping are 10 PSTHs, showing the average response for reaches to each target. By examining an individual PSTH, it is evident that this cell is responsive in the task: it has low baseline activity, then a vigorous response begins soon after the cue appears and is sustained through the delay period. Activity in this particular neuron diminishes by the time the movement begins. The neuron's spatial tuning is evident by examining all 10 PSTHs corresponding to a particular start configuration. For each of the four start configurations, spatial tuning is evident (more active for reaches to the left).

By comparing spatial tuning across the four start configurations, the influence of the eye and hand position on activity in this neuron are evident. Between the start configurations in the *top two panels,* the eye position (and therefore the eye-centered locations of the targets) is different, but the initial hand position (and thus the arm-centered locations of the targets) is the same. The neuron's spatial tuning is similar in these start configurations, which indicates that the cell is relatively insensitive to the location of the reach goal in eye-centered coordinates. In contrast, between the *bottom two panels,* the initial hand position is different, whereas the eye position is consistent. The spatial tuning of the neuron is markedly different between the two start configurations, indicating that the cell is sensitive to the location of the target in a limb-centered reference frame. In fact, it appears that the preferred reach endpoint may move along with the hand. Taken together, these four response profiles suggest that this cell encodes reach goals in arm-centered coordinates and not in eye-centered coordinates. Figure 4, *B—D,* illustrates three more apparently limb-centered neurons. In this plotting format, the average firing rate during the 500-ms delay period is depicted in grayscale. The 40 task conditions are plotted with the same spatial arrangement as in Fig. 4*A*.

Figure 5*A* depicts a neuron with a very different response pattern. As the initial eye position is shifted from the right to the left side of the touch point (*top 2 panels*), the response field moves (partially) along with the direction of gaze. However, when the initial hand position is changed (*lower 2 panels*), the spatial tuning is largely unaffected. This neuron is relatively insensitive to the hand-centered location of the targets but is highly sensitive to the eye-centered target location. This cell may use an eye-centered reference frame to represent reach targets. Figure 5, *B–D,* illustrates additional apparently eye-centered neurons.

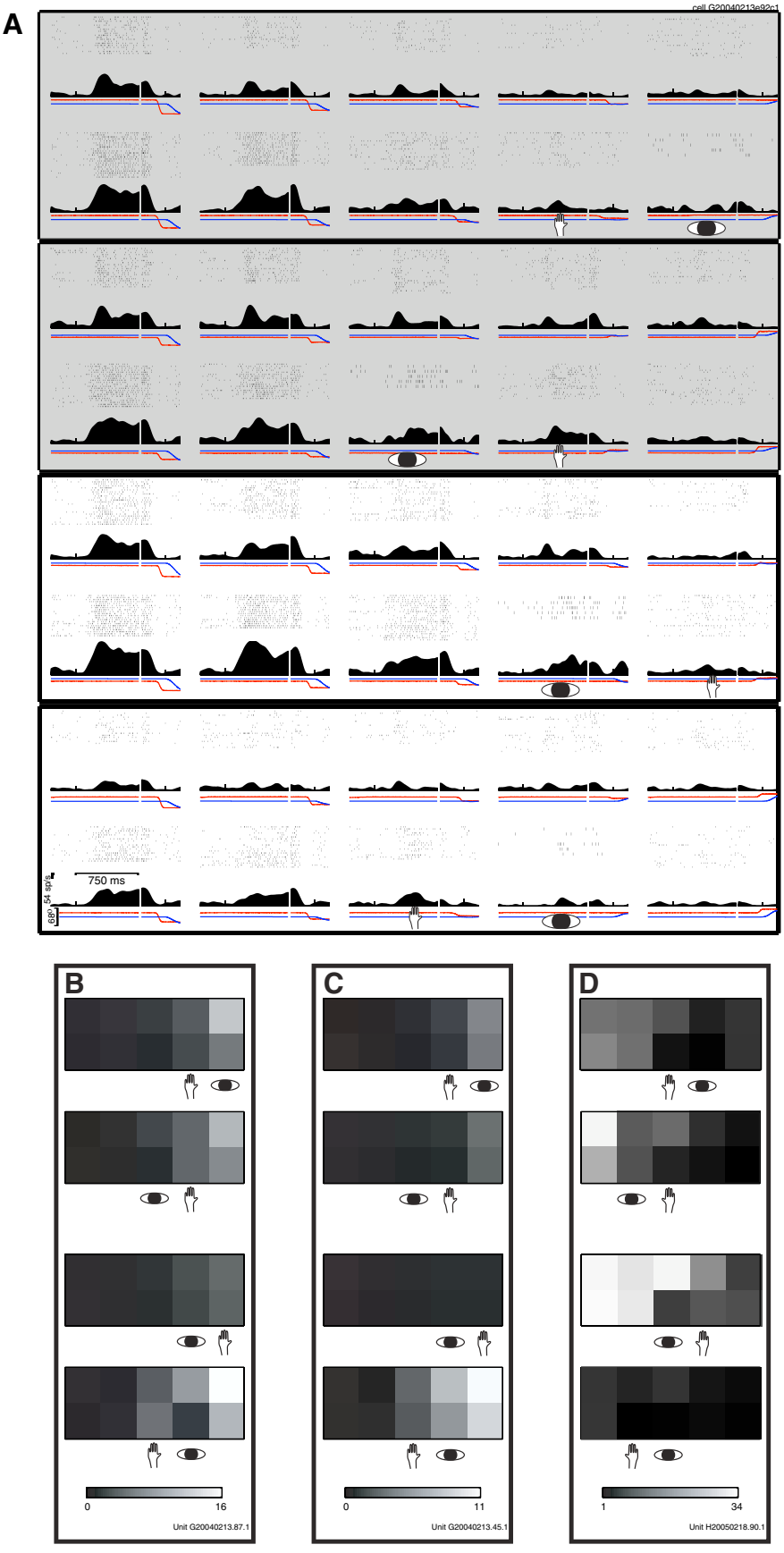

FIG. 4. PMd neurons that encode reach goals in arm-centered coordinates. *A*: each of the 4 panels shows neural responses for 1 start configuration. Within the panels, the 10 subpanels are positioned at the relative location of the corresponding reach target. Icons depict the initial hand and eye positions for that start configuration. Each subpanel shows, from top to bottom: rasters for all repetitions of the reach; peristimulus time histogram (PSTH; constructed by convolving rasters with a Gaussian kernel of SD = 30 ms, and summing); horizontal components of average eye position (red) and average hand position (blue). Data are aligned on the time of target appearance (left portion of the subplot) and the time of reach initiation (right portion). The 2 panels with a gray background indicate task configurations in which the initial hand position was held constant; the 2 panels with a white background indicate the task configurations when the eye position was held constant. *B–D*: 3 additional neurons. Average firing rate during the delay period is depicted by grayscale for each target location and start configuration. The distance values (plotted in Fig. 6) for these cells were as follows: neuron in *B*: x = sensitivity to eye position = 0.08, y = sensitivity to hand position = 0.30; neurons in *C*: x = 0.21, y = 0.46; and in *D*: x = 0.22, y = 0.61.

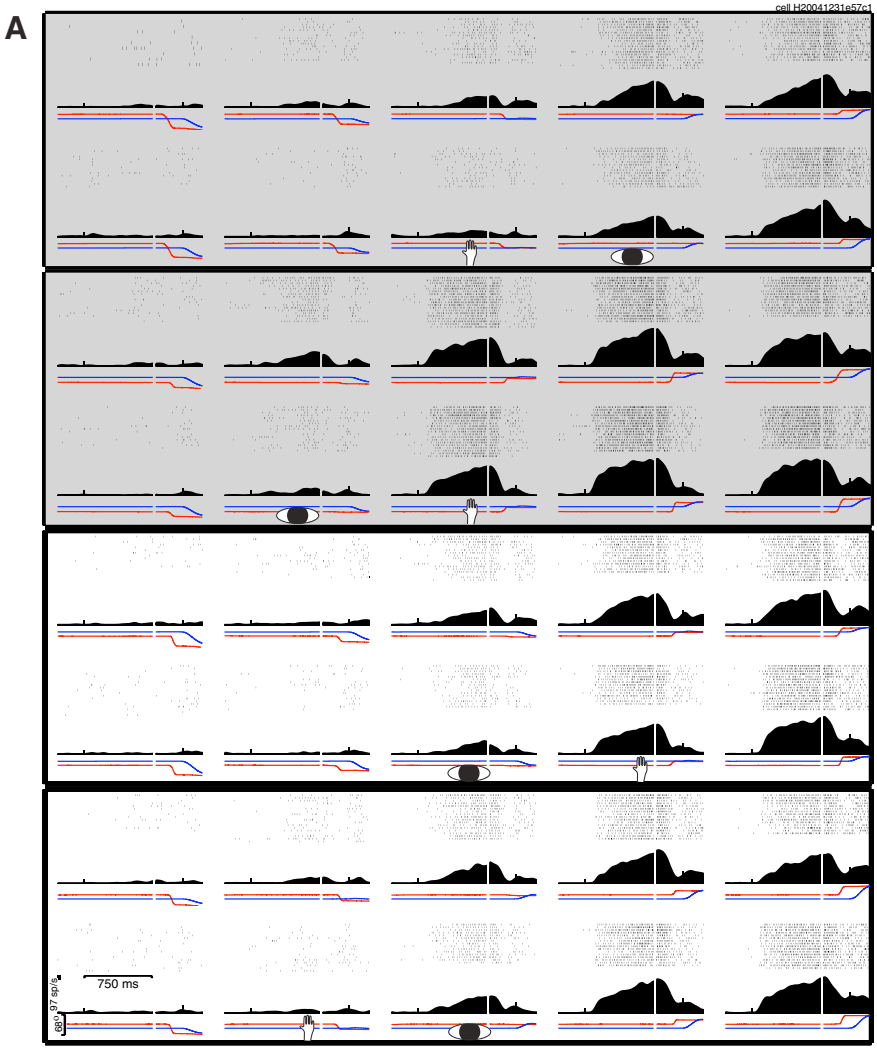

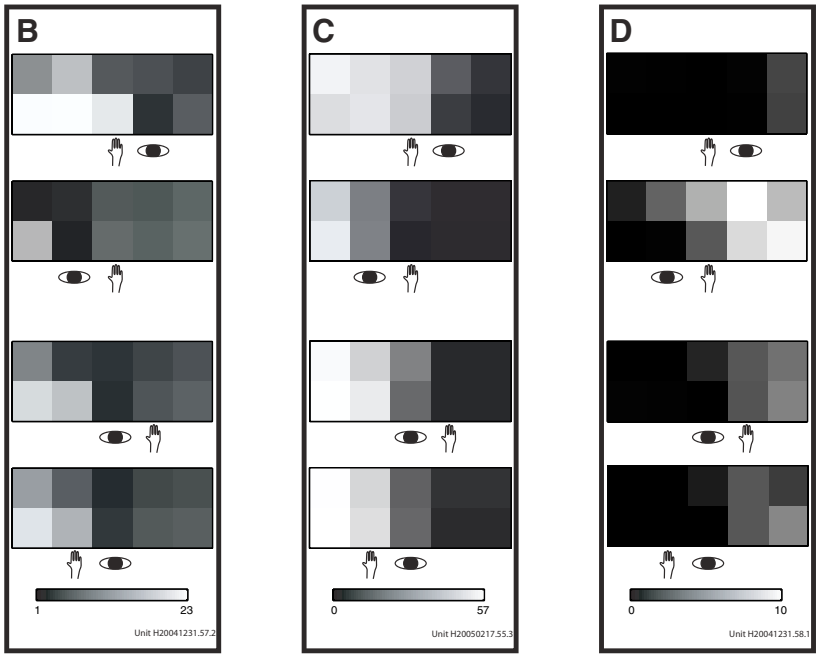

FIG. 5. PMd neurons that encode reach goals in eye-centered coordinates. See Fig. 4 legend for details. Distance values plotted in Fig. 6 were as follows: neuron in *B*: $x = 0.45$, $y = 0.07$; neuron in *C*: $x = 0.41$, $y = 0.07$; neuron in *D*: $x = 0.54$, $y = 0.11$.

The neurons depicted in Figs. 4 and 5 represent a small population of neurons in our dataset where a relatively clear reference frame was observed. We performed three population quantifications that convey the diversity of responses observed in PMd.

Population analysis 1: sensitivity

We directly compared the influence on PMd neurons of changing target locations relative to the eyes and relative to the arm. The 154 neurons tuned for target location are included in this analysis. For each neuron, we computed the Euclidean distance between the two response profiles collected with the hand at a consistent position but the eyes at different positions (i.e., start configurations i and ii in Fig. 2*B*) and compared that to the distance between the response profiles collected with the eyes at a consistent position and the hand at different positions (start configurations iii and iv in Fig. 2*B*). In Fig. 6, the two distances computed for each neuron are plotted against one another. A neuron that encodes reach goals in a strictly eye-centered reference frame would exhibit a large distance along the horizontal axis (sensitive to eye-centered target location) but a small distance along the vertical axis (insensitive to limb-centered target location) and thus would appear below the diagonal. Similarly, neurons plotted above the diagonal are more influenced by the target's location relative to the limb than by the target's location relative to the retina and might encode reach goals using a limb-centered reference frame.

Filled points indicate neurons the bootstrap-estimated confidence intervals of which do not cross the unity diagonal. For these neurons, we can assert with confidence that the neuron is more sensitive to the eye-centered (below the diagonal) or limb-centered (above the diagonal) position of the targets. (Note that this analysis sets upper limits on the number of eye- and limb-centered neurons; a greater sensitivity to arm position than eye position is a necessary but not sufficient condition to characterize a neuron as limb-centered.) Gray squares indicate, for each neuron, the average distance between two resampled versions of the same response profile (see METHODS). With noiseless neurons, these values would be zero.

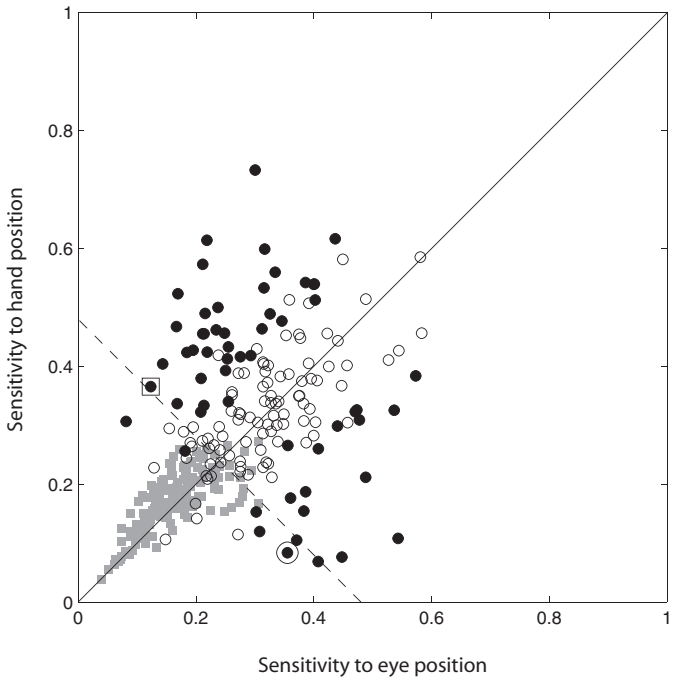

FIG. 6. Population quantification 1: sensitivity. Neurons that lie above the unity diagonal may employ limb-centered coordinates; neurons below the diagonal may use eye-centered coordinates. Filled symbols indicate neurons the confidence intervals of which do not cross the unity diagonal. The square surrounds the point corresponding to the neuron in Fig. 4*A*; the ring surrounds the neuron in Fig. 5*A*. Gray squares illustrate noise in the measurement about a true value of 0 for each neuron. Dashed line indicates the border that includes 95% of the gray squares.

We can use this analysis as a basis to divide the neural population into four categories: neurons that might encode reach goals in limb-centered coordinates lie above the diagonal with confidence intervals that do not cross the diagonal (39 cells). Neurons that might encode reach goals in eye-centered coordinates lie below the diagonal with confidence intervals that do not cross the diagonal (19 cells).

The remaining 96 neurons exhibited confidence intervals that crossed the unity diagonal (hollow symbols in Fig. 6), and thus the influences of the eye position and hand position on these neurons were not statistically distinguishable. These cells were ascribed to two categories based on the magnitude of their distance metrics.

Neurons that might encode reach goals in head-centered coordinates would be unaffected by either the eye or hand position. Such cells would exhibit small distance values between both pairs of response profiles. We identified these neurons as lying within a boundary determined from the estimate of measurement noise in the distance metric (see METHODS). There were 15 potential head-centered neurons.

The fourth category contained neurons that were sensitive to both the eye- and limb-centered locations of the targets; these neurons exhibited sensitivities to both the eye and hand position that were large but not statistically different from each other. The majority of neurons (81 cells) fall into this "unclassifiable" category.

We sought to ascertain a reference frame for these unclassifiable neurons. It has recently been shown that some reach-related neurons encode reach goals in a reference frame defined by the relative position of the eyes and hand. Such neurons have been found in parietal area 5 by Buneo et al. (2002) and in a region of PMd rostral to our recording sites (Pesaran et al. 2006). Because our unclassifiable neurons were sensitive to both the eye- and limb-centered locations of reach goals, it could be that they employ a combined eye+hand reference frame. To test this, we compared each neuron's minimal distance in either eye- or limb-centered coordinates to its minimal distance in a combined eye+hand reference frame. Figure 7*A* exhibits this comparison. Eight neurons exhibited a reliably better alignment in a combined eye+hand reference frame (filled points below the unity diagonal), whereas seven were reliably better aligned relative to the eyes or hand alone (filled points above the diagonal). Using this metric, we estimate that 53% of neurons in the portion of PMd where we recorded are better described as using a reference frame defined by the relative position of the eyes and hand than by a reference defined by the position of either the eyes or arm alone.

Points in Fig. 7*A* are color-coded according to their categorization in Fig. 6: cells that were reliably below the diagonal in Fig. 6 (that is, eye centered) are red in Fig. 7*A*; neurons that

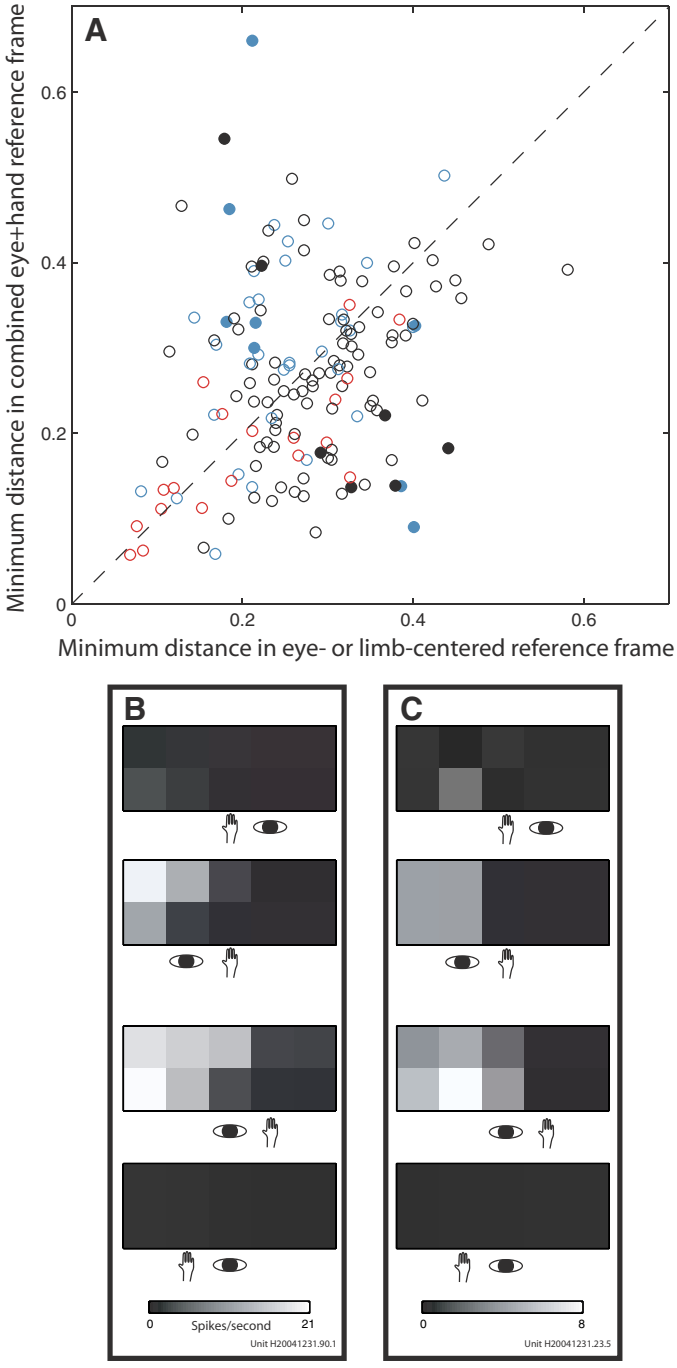

FIG. 7. Evidence for a combined eye+hand reference frame. *A*: neurons plotted below the diagonal are better-aligned in a reference frame defined by the relative position of the eyes and hand than in either an eye- or hand-centered reference frame. Filled points indicate neurons the confidence intervals of which do not cross the unity diagonal. Colors indicate placement of neurons in Fig. 6. Red points: neurons significantly more sensitive to eye position (filled points below the diagonal in Fig. 6). Blue points: neurons significantly more sensitive to hand position (filled points above the diagonal in Fig. 6). Black points: neurons with statistically indistinguishable sensitivities to eye or hand position (unfilled points in Fig. 6). Note that the axes have been truncated to the extent of the data for visual clarity. *B* and *C*: 2 neurons that encode target locations relative to the combined position of the eyes and hand. Their locations in *A* are as follows. Neuron in *B*: $x = 0.40$, $y = 0.09$. Neuron in *C*: $x = 0.44$, $y = 0.18$.

were reliably above the diagonal in Fig. 6 (limb-centered) are blue in Fig. 7*A*; neurons that could not be classified as eye- or limb-centered in Fig. 6 are black in Fig. 7*A*. These neurons were the best candidates for using a relative position reference frame because they did not exhibit either an eye- or a limb-centered reference frame. Several of these neurons (5 of 7), which had been labeled unclassifiable, were better characterized as using an eye+hand reference frame than either an eye- or limb-centered reference frame. In contrast, few neurons formerly classified as limb- or eye-centered were better characterized as employing a combined eye+hand reference frame (3 of 8). Figure 7, *B* and *C,* illustrates individual neurons that appear to encode target locations relative to the combined position of the eyes and hand: they are more active when the hand is to the right of the eyes, and the response field moves in tandem with the eyes and hand together.

The sensitivity analysis shows that there exist within PMd small populations of neurons that appear to encode reach goals in reference frames that are limb-centered, eye-centered, and defined by the relative position of the eyes and hand. However, the largest population of neurons in PMd is influenced by the positions of both the eye and arm, albeit apparently not in any spatially organized manner.

Population analysis 2: best shift

Reference frame analyses commonly involve shifting tuning curves until the optimal alignment between them is found (Bradley et al. 1996; Shenoy et al. 1999). Here such an analysis permits us to test whether neurons employ an eye-centered reference frame or an extrinsic hand-centered reference frame. Note that because a hand-centered reference frame is only one of several possible limb-centered reference frames, this analysis probably underestimates the number of neuron with limb-centered reference frames in PMd; this point is treated more fully in the DISCUSSION.

For each of the 154 neurons that were tuned for reach target location, two best shifts were determined: the shift that maximized the correlation between the two response profiles collected with a common initial hand position (start configurations i and ii), and the shift that maximized the correlation between the two response profiles collected with a common eye position (start configurations iii and iv). Figure 8, *A* and *B,* shows histograms of the optimal shifts for each pair of response profiles.

As in the sensitivity analysis, four categories of neurons were defined. A neuron that employed a hand-centered reference frame would exhibit an optimal shift of 0 between the two hand-aligned response profiles and an optimal shift of 1 or 2 between the two eye-aligned response profiles. A neuron with an eye-centered reference frame would exhibit an optimal shift of 1 or 2 between the two hand-aligned response profiles and an optimal shift of 0 between the two eye-aligned response profiles. Neurons that were insensitive to the eye- and hand-centered position of reach goals (e.g., head-centered) would exhibit optimal shifts of 0 in both cases. Neurons with optimal shifts of 1 or 2 in both cases are influenced by both eye and hand position in a complex manner.

By these criteria, there are 44 neurons that encode reach goals in a hand-centered reference frame, 24 that encode reach goals in eye-centered reference frames, 9 neurons that appear

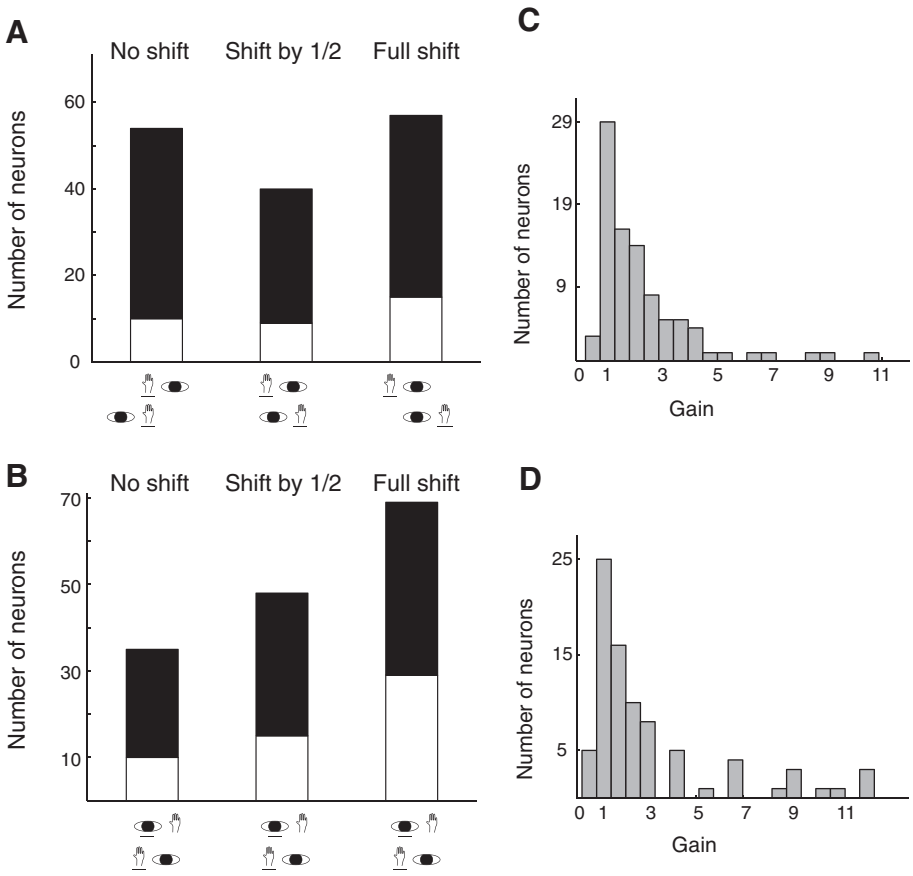

FIG. 8. Population quantification 2: best shifts. *A*: histogram of optimal shifts between response profiles measured in start configurations i and ii (common initial hand position). The underlining indicates the same actual location on the screen. *B*: optimal shifts between start configurations iii and iv. Shading of histograms indicate each neurons' position in the other histogram: neurons shown in white exhibit a best correlation when unshifted in the other histogram; neurons shown in black exhibit a best correlation at a partial or full shift in the other histogram. *C* and *D*: histogram of gains computed at optimal shift determined in *A* and *B*.

insensitive to both the hand- and eye-centered locations of the reach goals, and 77 neurons that exhibit complex properties.

We also measured the gain effect due to changing the eye and/or hand position at the optimal shifts (Fig. 8, *C* and *D*). The modal gain was 1 in both cases. The distributions of gains were not significantly different from each other (Mann-Whitney test, $P < 0.05$).

Population analysis 3: decode

Which reference frames are discriminable from one another in the PMd population response? We asked whether an ideal observer could determine the target location and start configuration presented to the animal on an individual trial by examining the distribution of neural activity across the population for that trial. Figure 9 illustrates the outcome of this analysis. All 212 neurons responsive in the task were included in this analysis. The confusion matrix shows the instructed task geometry (target location and start configuration) along the horizontal axis, and the decoded task geometry along the vertical axis. Trials that plot along the unity diagonal are those for which the actual target and start configuration were correctly estimated from the population response. The pattern of errors in estimating start configuration reveal in which reference frames PMd conveys information.

Considering *monkey H* (Fig. 9*A*) the start configuration is estimated correctly 73% of the time (470 of 640 trials). If PMd as a whole was insensitive to the position of the hand, then start configurations iii and iv would not be distinguishable based on the population of neural activity. In fact, these two start configurations were confused for one another in only two trials. Similarly, if eye position did not influence PMd activity, then start configurations i and ii would be confused with one another on half the trials. This confusion occurred in 14 trials. Thus PMd conveys information about the direction of gaze, albeit to a somewhat lesser extent than the position of the hand. Results were similar in *monkey G* (Fig. 9*B*): start configuration was estimated correctly 67% of the time (698 of 1,040 trials). One hand position was confused with the other in 14 trials (1%), and one eye position was confused with the other in 63 trials (6% of trials).

Apart from the concentration of trials along the main diagonal, perhaps the most salient feature in Fig. 9 is the pattern of banding parallel to the main diagonal. This shows that start configurations i and iv tend to be confused for one another, whereas start configurations ii and iii tend to be confused for one another. These pairs of start configurations have the same relative position between the eyes and the hand (hand left of eyes for configurations i and iv; hand right of eyes for configurations ii and iii) Thus confusions within these pairs indicate the presence of a reference frame in the PMd population defined by the combined position of the eyes and hand and insensitive to the position of the eyes and hand relative to the body. For *monkey H,* in 21% of the trials, the true start configuration is confused with the one that shares a relative hand and eye position. For *monkey G,* 18% of trials resulted in confusions between start configurations that share a relative hand and eye position. If PMd was sensitive to the position of the eyes and hand relative to one another but insensitive to their position relative to the body, then start configurations i and iv

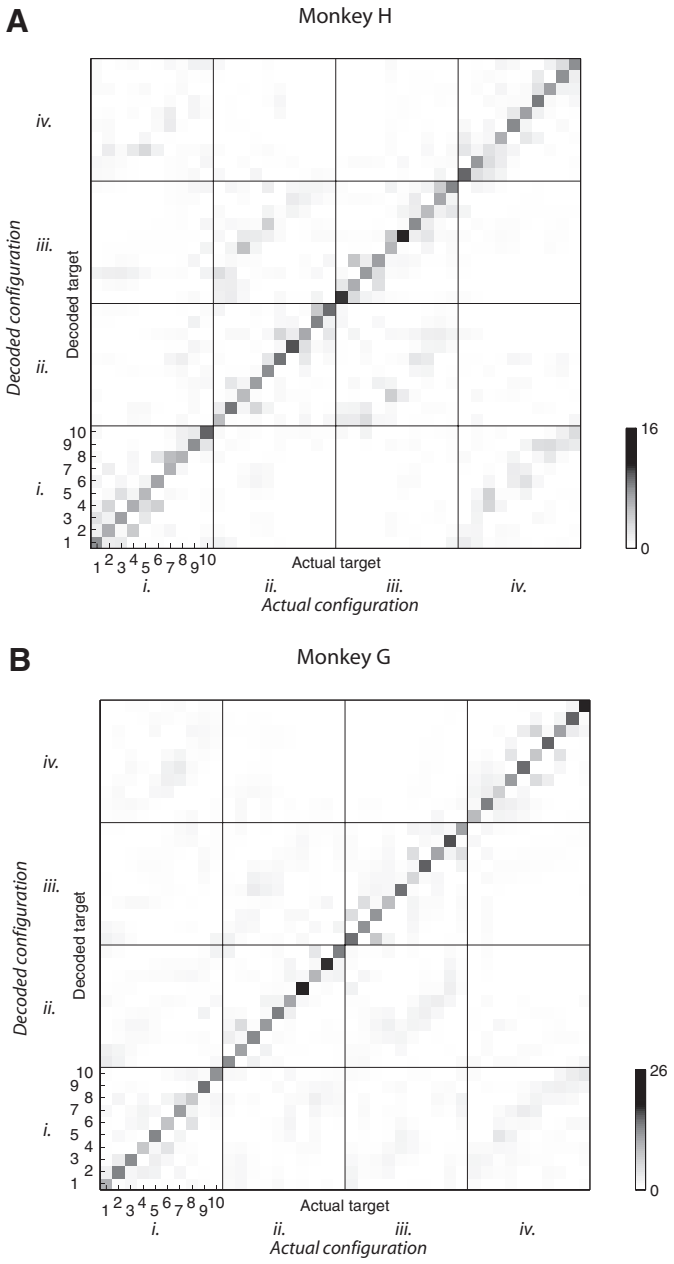

FIG. 9. Population quantification 3: decoding. Confusion matrices depict the number of trials that exhibited each of the possible combinations of actual and decoded target location.

(likewise, ii and iii) would be confused for one another in 50% of trials.

All of these trends persist when target location is decoded as well as start configuration, although overall percents correct decrease (46% of trials correctly decoded for *monkey H* and 47% for *monkey G*)

Examples of unclassifiable neurons

Figure 10 illustrates the diversity of responses observed within PMd. These cells exhibit spatial tuning with no obvious consistency among the four different response profiles. They are influenced by the position of the eyes and hand but in complex ways that precluded their categorization into the reference frames we tested.

Topographic distribution of reference frames

Do adjacent neurons exhibit similar reference frames in PMd? The anatomical locations of the 73 neurons that were

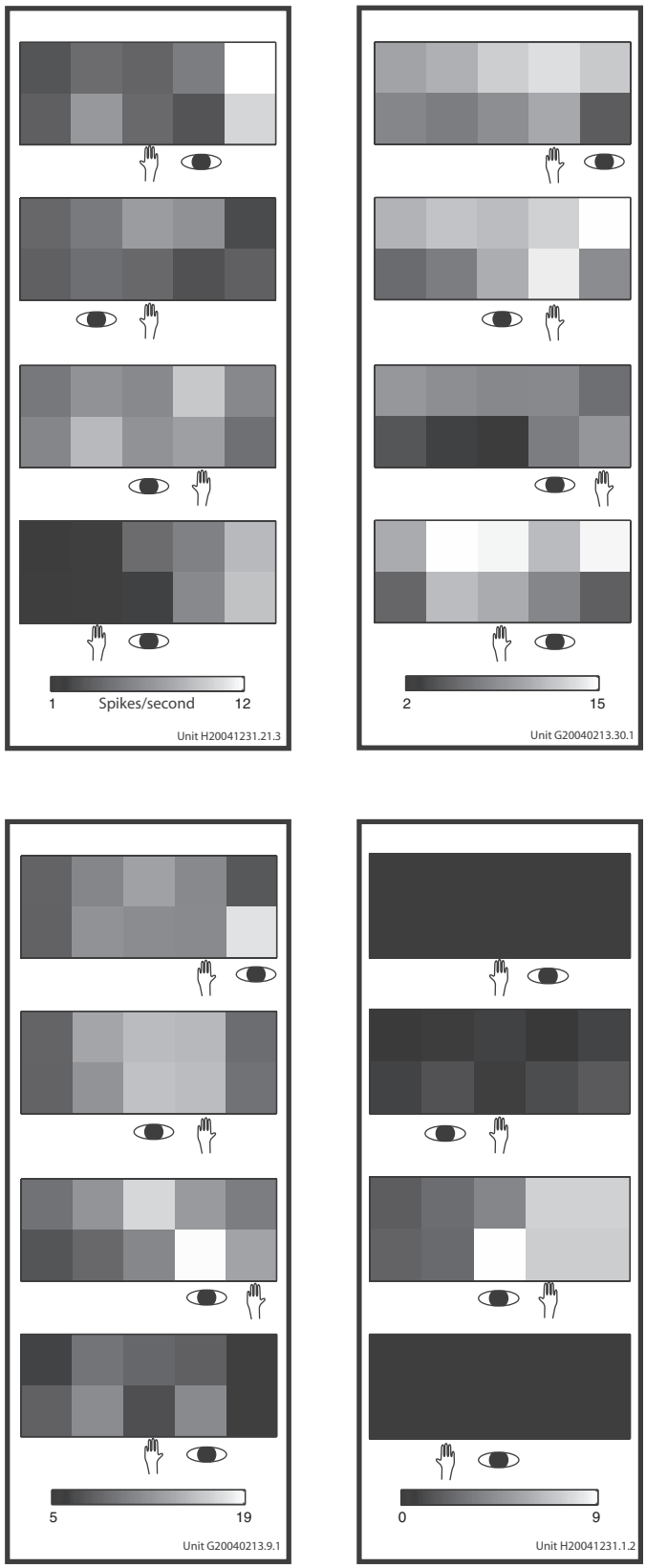

FIG. 10. Some PMd neurons without discernible reference frames.

more influenced by either eye- or hand-centered target location (those plotted with filled symbols in Fig. 6) are plotted in Fig. 11. The color scale indicates the number of neurons that were significantly more sensitive to eye or hand position on each electrode. Evidence for topography is not strong, but some trends are arguably visible. First, there might be a trend for neurons that employ a particular reference frame to cluster. Nearby electrodes tended to record from neurons with the same reference frame. There were no electrodes where both eye- and hand-centered neurons were found. Second, there may be a trend for the candidate eye-centered neurons to be closer to the spur of the arcuate sulcus. Finally, there may be a trend for limb-centered neurons to be more posterior (closer to primary motor cortex.)

Behavior

From these data, it appears that the same reach can be accompanied by very different patterns of delay period activity in PMd because PMd responses depend on the direction of gaze. However, it is also possible that different directions of gaze induce slight differences in the metrics of the reach. Perhaps differences in the reach can account for the differences we observed in neural responses.

First we examined how the direction of gaze affected the parameters of the reach. Endpoint, trajectory, reaction time, movement duration, and peak velocity were examined (Fig. 12). This comparison was performed between start configurations i and ii, where eye position differed so that the instructed start and endpoints of the reaches were held constant. Figure 12*A* shows the distribution of endpoints for both fixation positions. (Data from 1 dataset for each monkey were analyzed; the day for which the most trials were performed.) For the two different fixation positions, the distribution of reach endpoints differed for 9 of 10 targets (for *monkey G*) and 7 of 10 targets for (*monkey H*) in the horizontal and/or vertical components (Wilcoxon rank sum test, $P < 0.05$). The average separation between the mean endpoints under the two different starting eye positions was 3 mm for both monkeys. This is small compared with the average length of the reaches (136 mm).

Figure 12*B* shows the trajectories of all reaches to targets in the upper row, for both fixation positions. The distribution of hand paths is highly overlapping, but trajectories show a tendency to be biased in the direction of the fixation point.

Peak velocity of the reach also depended somewhat on eye position. For *monkey G,* the distributions of peak velocities

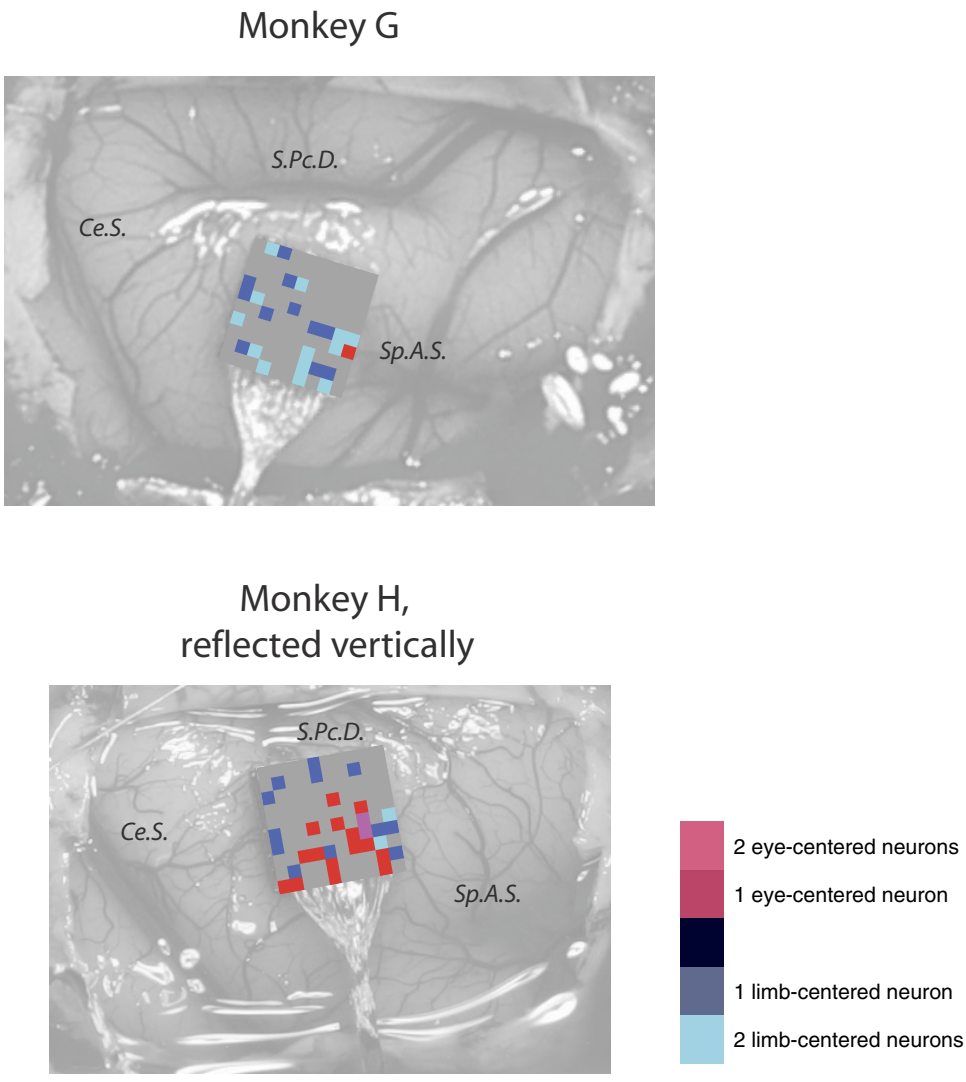

FIG. 11. Anatomical distribution of reference frames. Abbreviations of sulci as in Fig. 1.

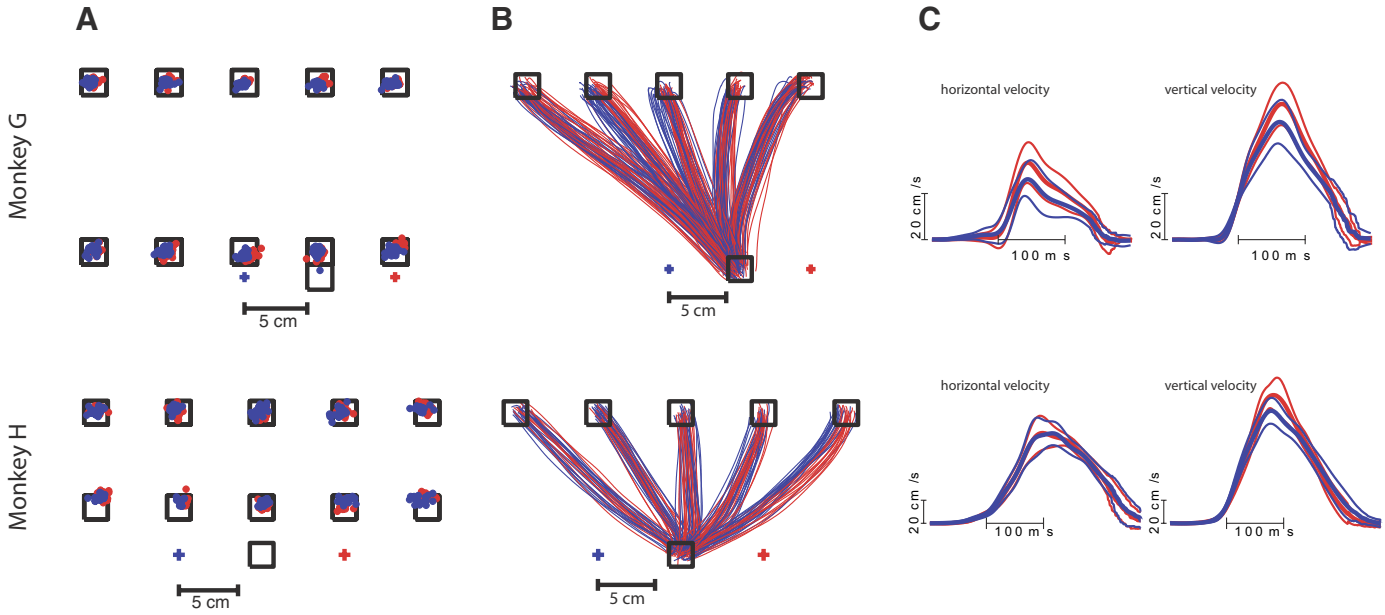

FIG. 12. Behavior. *Top row: monkey G. Bottom row: monkey H. A*: endpoints for reaches to all 10 targets for 2 different fixation positions. Touch point, fixation points, and targets are drawn to scale. *B*: reach trajectories for 2 different fixation positions. Hand paths for reaches to the upper row of targets is shown for fixation to the right (red) and left (blue). *C*: horizontal (*left*) and vertical (*right*) components of velocity for reaches to 1 target. Means ± SD are shown. Within each plot, average velocity when fixation is to the right is shown in red, and average velocity when fixation is to the left is in blue. *Top 2 panels: monkey G* reaches to rightmost target in upper row. This is 1 of 5 targets for which peak reach velocity differed significantly (*t*-test, $P < 0.05$) between the 2 start configurations. *Bottom 2 panels: monkey H* reaches to rightmost target in lower row. This is 1 of 2 targets for which peak velocity differed significantly. Traces are aligned to the beginning of the reach. The left edge of the horizontal scale bar indicates this time.

differed significantly (for horizontal and/or vertical velocities) between the two start configurations for 5 of the 10 target locations (*t*-test, $P < 0.05$). For *monkey H,* peak velocities were significantly different for reaches to 2 of the 10 targets (*t*-test, $P < 0.05$; horizontal component only was different in both cases). Figure 12*C* plots the mean (±SD) velocity (horizontal components on the *left,* vertical components on the *right*) for reaches to one target for each monkey. Velocities are shown for reaches to two of the targets where there was a significant difference in the peak velocities between the two start configurations. The *top panel* shows average velocity traces for *monkey G*'s reaches to the far right target in the lower row, where peak velocities differ significantly for both components of the reach. Velocity profiles for fixation to the right are shown in red, and profiles for fixation to the left are shown in blue. The *bottom panel* shows averaged velocity traces for *monkey H*'s reaches to the far right target in the upper row, where peak velocities differ significantly for the horizontal component. Note that this velocity increase may be secondary to the slightly longer trajectory when fixation is to the right.

Thus the direction of gaze did induce small differences in reach behavior. We explored whether the differences in movement parameters are sufficient to account for the large differences in neural activity evident between different start configurations.

We focused our analysis on reach endpoint. Figure 13*A* explains the analysis (see METHODS), for one example neuron (the cell in Fig. 5*A*). Briefly, firing rate is regressed against instructed endpoint for one fixation configuration. The greatest separation between mean endpoints is converted into expected firing rates due to differences in endpoint under the two fixation positions. The ratio between this expected difference in firing rate due to differences in endpoint and the actual difference in firing rate between the two start configurations for reaches to that target is computed. The ratio indicates the fraction of the firing rate difference that can be accounted for by the difference in endpoint. The remaining portion is at least partially due to the difference in eye-centered location of the target.

Figure 13*B* plots a histogram of this ratio, for each neuron that was analyzed ($n = 164$, both monkeys, 1 day per animal. All neurons were included, without employing the 3 spikes/s firing rate threshold enforced in all other analyses.) Ten neurons exhibited ratios that were infinite because the difference in firing rate for the two different eye positions was zero. The difference in firing rate for the two different reach endpoints accounts for 14% of the difference in firing rate for the two fixation positions, on average (averaged over the 154 neurons for which the ratio is finite). For 75% of neurons, the ratio is <0.1, meaning for these neurons, $<10\%$ of the difference in firing rate between the two fixation configurations is due to differences in the actual reach endpoint.

Thus as a whole, the small differences in reach endpoint under the two different fixation positions cannot account for the large differences in firing rate observed between them. Firing rate differences are likely due instead to the differences in the eye-centered locations of the targets.

DISCUSSION

We observed that the retinal location of reach goals influenced reach preparatory activity in PMd. Neurons were influenced by eye and hand position in a variety of ways, and as such, a diversity of reference frames was observed among PMd neurons. We observed some neurons with limb-centered reference frames and others with eye-centered reference frames. We

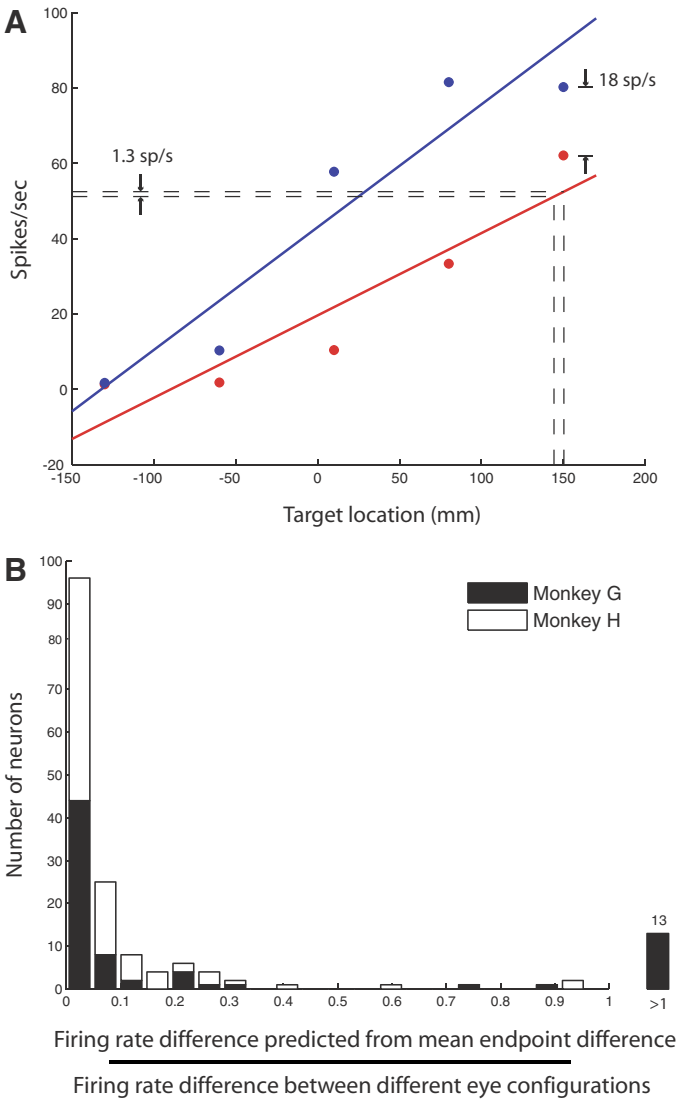

FIG. 13. Difference in reach endpoint cannot account for differences in firing rate. *A*: details of the analysis for 1 cell (same neuron as in Fig. 5*A*). Red points indicate average firing preceding reaches to targets along the bottom row of targets for fixation to the right. Red line is the regression fit. Blue points and line indicate firing rates preceding the same reaches when fixation is to the left. Dashed vertical lines indicate the mean endpoints for reaches to the rightmost target for the 2 fixation positions. Dashed horizontal lines indicate the expected firing rates before reaches to those endpoints, predicted by the linear regression. For this cell, a firing rate difference of 1.3 spike/s is expected, based on the difference in behavior. In contrast, the actual firing rate difference between these 2 fixation conditions is 18 spike/s. The ratio between the expected and actual values is 0.07. *B*: histogram of ratios of expected to actual firing rate difference for all neurons. Thirteen neurons exhibited a ratio >1. Three of them have finite ratios >1 (1.5, 2.5, and 5.8), and 10 have infinite ratios.

also observed neurons that appear to encode reach goals relative to the combined position of the eyes and hand. However, the largest single category of neurons we observed was unclassifiable: cells that exhibited spatial tuning that changed in complex ways as the eyes and hand moved (e.g., Fig. 10). For these neurons, there appeared to be no consistent relationship between the response fields measured in each of the four start configurations. It is possible that these cells might exhibit a reference frame in some space that we did not test, such as an intrinsic space (e.g., joint angles), or perhaps in a region of extrinsic space (e.g., in depth or lower frontoparallel space). It is also possible that these neurons might have no reference frame: they might exhibit response fields that change location and shape depending on the position of the eyes and hand but bear no consistent relationship to either or both. Given PMd's close involvement in the control of arm movements, we infer that this surprisingly complex encoding scheme may be an efficient strategy for specifying reach goals (Deneve et al. 2001; Pouget and Snyder 2000; Wu and Hatsopoulos 2007).

Correspondence between the analyses

We employed three separate population quantifications. Two of them (the sensitivity and shift analyses) tested reference frames in single neurons, and the third examined which reference frames were distinguishable in a population of simultaneously recorded neurons. The three corroborate each other: PMd neurons are influenced by the direction of gaze in addition to the position of the hand. The location of the target relative to the arm is encoded somewhat more strongly in PMd activity than is the target's location relative to the direction of gaze.

The sensitivity and shift analyses address different questions. The sensitivity analysis directly compared the influence on neural activity of the initial hand position and the eye position. The shift analysis is a common technique in reference frame studies and is appropriate for distinguishing between some reference frames, for example eye-centered versus head-centered (as in Bradley et al. 1996), because both candidate reference frames are extrinsic and unique. However, it is less appropriate for distinguishing between eye- and limb-centered reference frames. This is because although there are only a small number of eye-centered reference frames (chiefly, retinal, binocular cyclopean, and oculomotor), there is a multitude of limb-centered reference frames that the brain could potentially employ to encode reach goals (for example, neurons with hand-, elbow-, and shoulder-centered reference frames have been reported). These reference frames are defined in either extrinsic (that is, external space relative to a body part) or intrinsic (that is, in the space defined by joint rotations or muscle activations) coordinates. When the eyes move from one position to another, virtually all possible eye-centered reference frames would move in tandem with the eyes; but when the hand moves from one position to another, only one limb-centered reference frame (hand-centered) would move in tandem with the hand. Furthermore, whereas neurons that employ an extrinsic eye-centered reference frame are well known to exist (in the retina, lateral geniculate nucleus and primary visual cortex, at very least), the existence of neurons that employ an extrinsic hand-centered reference frame have not been unequivocally demonstrated, nor are they necessary on theoretical grounds (Pouget et al. 2002). Thus analyzing reference frames by shifting response fields to find their optimal alignment offers a direct comparison between extrinsic eye-centered and extrinsic hand-centered reference frames: the prevalent eye-centered reference frame and perhaps the least plausible limb-centered reference frame. For this reason, we believe the shift analysis does not offer an unbiased comparison between limb- and eye-centered reference frames; this is why we emphasize the sensitivity analysis in this report.

It has been known since at least the work of Zipser and Andersen (1988) that reference frames manifested in a popu-

lation of neurons can be different from those evident in any component neuron. The third analysis, decoding, yielded a population view of the reference frames present in PMd. It confirmed that PMd as a whole conveys information about the position of the hand, the direction of gaze, and the location of the target, because all these factors can be estimated from activity in the neural population.

Head-centered reference frames in PMd?

Our experimental design would have revealed neurons that were insensitive to target locations relative to either the eyes or arm. Such cells are candidate head-centered neurons. (They could also be body- or world-centered: these were not distinguishable from head-centered in our experiment because the head and body were not moved.) Two of the three population analyses identified candidate head-centered neurons (15 in the sensitivity analysis, 9 in the shift analysis.) However, when inspecting the PSTHs for these candidate cells, we observed no neurons with head-centered reference frames.

Although we found very little evidence for neurons that encode reach goals in a purely head-centered reference frame, we predict at least some PMd neurons will be modulated by changing head position as is the case in PMv (Graziano et al. 1997a). Such neurons could support a body-centered representation of target location at the population level (Snyder et al. 1998). Similarly, various other postural signals beyond those we tested may influence PMd neurons.

Relation to prior studies

Several other studies have investigated the reference frame for reaching in PMd. The initial study of reference frames in PMd Caminiti et al. (1991) concluded that PMd encodes reach goals in shoulder-centered coordinates. However, eye position was not monitored in that study. Thus the contribution of the retinal location of reach goals to spatial coding in PMd was not explored.

Since then, other groups have studied retinal and eye position influences on PMd neurons (Boussaoud 1995; Boussaoud et al. 1998; Cisek and Kalaska 2002; Pesaran et al. 2006). There are discrepancies between the studies regarding the degree to which eye position influences PMd neurons.

In the studies by Boussaoud and colleagues, target locations were changed relative to both the eyes and the hand together. Thus although those authors attributed the differences in firing rate they observed to the changes in the retinal locations of the targets, their study could not rule out that the firing rate differences could also be due to changes in the limb-centered locations of the targets. Our experimental design dissociated limb- and eye-centered target locations.

Cisek and Kalaska (2002) reported a small modulation with eye position in PMd, and a stronger modulation with hand position. In our study, effects of eye position were more comparable to the effects of hand position. Monkeys in the Cisek and Kalaska study were trained to control their hand position to fulfill task requirements but were not trained to control their eye position. In our study, eye and hand position were treated symmetrically, affording a direct comparison between the two. It may be that PMd neurons use reference frames that are anchored to whichever body parts are most stable during the task; if so, in their study, reference frames would be predominantly limb-centered because only the hand was under task control, whereas in our study, reference frames could be both eye- and limb-centered. The notion that the brain might preferentially use the most reliable signals to guide behavior has recently received both psychophysical (Sober and Sabes 2005) and theoretical (Deneve et al. 2007) support.

In the study of Pesaran et al. (2006), it was determined that PMd encodes the relative position of the eyes, hand, and target and is largely invariant to their position relative to the body and world. Our study employed a highly similar experimental paradigm, which affords a fairly direct comparison between the studies. We identified a subpopulation of neurons that employed a relative position code (filled points below the diagonal in Fig. 7*A*). However, the modest proportion of neurons that we observed with this property is probably not sufficient to support the notion that this is the principal encoding scheme used by PMd. Relative position coding was also manifested in the discriminability of task geometries in the population activity. In our decode analysis, we found that on 18–21% of trials the population response was misidentified as indicating that the eye and hand were in the correct position relative to one another but at the wrong position relative to the head and torso. If PMd employed only a relative position code, then this misidentification would have occurred on ~50% of trials. Thus there is more information present in PMd than a relative position code alone could provide: information about the position of the hand and eyes relative to the body can be extracted from the population response in PMd. We expect that with larger neural populations, the misidentifications of the position of the eyes and hand relative to the body would only be further reduced.

Another difference between the various PMd studies is the recording sites. Our arrays were positioned caudal to the spur of the arcuate sulcus, in the region of PMd with the densest projection to the spinal cord and primary motor cortex (Dum and Strick 1991). Caminiti et al. (1991) and Boussaoud et al. (1998) apparently recorded from regions partially overlapping with ours sites. Cisek and Kalaska (2002) and Pesaran et al. (2006) recorded from sites that appear to be just medial to and perhaps rostral to the caudal tip of the arcuate sulcus. This zone, termed pre-PMd by Picard and Strick (2001), is densely interconnected with the prefrontal cortex (Lu et al. 1994) but not directly connected with the primary motor cortex and spinal cord (Dum and Strick 1991; He et al. 1993; Lu et al. 1994). Projected onto the brains of our monkeys, these sites would be ~4 mm rostral to our arrays. It appears sensible that a relative position code would be found in this rostral region—its interconnections with the prefrontal cortex implicate the area in a higher-order encoding of movement endpoints—whereas a more heterogeneous reference frame—which includes information about the position of the hand relative to the body—is found in the more caudal area where we recorded because neurons there contribute more directly to controlling arm movements.

Caveats

We attempted to design a behavioral task that was similar to natural behaviors, while still providing an incisive dissociation of the various signals that may drive neurons. Nevertheless,

caveats apply. First, our observations were made while monkeys performed a highly trained task. Although our observations may extend to less restrained behaviors and to the perimovement epoch, it is also possible that they may not. Second, because eye position was unrestrained after the "go" cue in our task, as in natural movements, it is possible that saccade plans contribute to the signals we observed. To rule out this possibility would require training monkeys to form a saccade plan simultaneously with, and oppositely directed to, the reach plan (Snyder et al. 1997).

General considerations

Brain areas that employ a single reference frame are perhaps comparatively rare: Unitary reference frames might be expected chiefly in brain areas that are close to the sensory input, where neurons may encode stimuli in the reference frame of the sensory modality. For example, PRR encodes reach goals in an eye-centered reference frame, presumably because it receives a dominant input from the extrastriate visual cortex. However, we posit that most central areas are likely to contain a variety of reference frames as this may well provide the most effective control mechanism for arm movements.

We were surprised to discover that the eye-centered location of the reach goal exerts a powerful influence on reach planning activity in PMd because PMd is fairly close to the motor output for reaching and because the parameters of the reaches are far less sensitive to the direction of gaze than are PMd neurons. Future research must explore when and how eye signals are eradicated from the reach control pathway downstream from PMd. There are at least three possibilities. First, there may be a selective projection from PMd to M1 and the spinal cord: only the neurons that are not influenced by eye position might synapse downstream. Second, there might be a balanced projection, such that eye signals cancel in downstream neurons. The third possibility is that this cancellation only happens in the reach itself; indeed, eye-position signals have been reported in the EMG responses during reaching (cf. Fig. 5 in Boussaoud et al. 1998). There may be a functional benefit to the eye-position signals in PMd and elsewhere in the reach pathway: because hand and eye movements are normally tightly orchestrated, neurons that code reach plans in eye-centered coordinates or combined eye+hand coordinates might play a role in coordinating the two effector systems (Batista et al. 1999; Pesaran et al. 2006).

In summary, we found many neurons in PMd were sensitive to all of the variables we tested: target location, hand position, and direction of gaze. Many neurons did not exhibit spatial tuning that was consistent across different eye and hand positions or combinations of them. We expect other postural signals, such as head position or body orientation, will influence PMd as well. For a neuron to exhibit a reference frame, it would have to show a consistent spatial relationship to one (or a combination) of body parts, with others exerting less of an influence. For half or more neurons in our dataset, this was not the case. The constraint placed on PMd and associated brain areas is that a population of neurons must act together to guide a movement accurately; there is of course no requirement that those neurons employ a spatial coding strategy that is well-described by a reference frame. Neurons like those in our study for which we could not identify a reference frame may truly have no reference frame.

ACKNOWLEDGMENTS

We thank M. Churchland for valuable discussions throughout this project. We thank M. Howard for expert surgical assistance and veterinary care and N. Hatsopoulos for expert surgical assistance (*monkey G* implant).

Present address for A. P. Batista: Department of Bioengineering and Center for Neural Basis of Cognition, University of Pittsburgh, Pittsburgh, PA.

GRANTS

This study was supported by Burroughs Wellcome Fund Career Awards in the Biomedical Sciences to A. P. Batista and K. V. Shenoy, National Defense Science and Engineering Graduate Fellowships to G. Santhanan and B. M. Yu, National Science Foundation Graduate Research Fellowships to G. Santhanam and B. M. Yu, the Christopher Reeve Paralysis Foundation to S. I. Ryu and K. V. Shenoy, a Stanford University Bio-X Fellowship and the National Institutes of Health Medical Scientist Training Program to A. Afshar, and the following awards to K. V. Shenoy: the Stanford Center for Integrated Systems, the NSF Center for Neuromorphic Systems Engineering at Caltech, Office of Naval Research, the Sloan Foundation and the Whitaker Foundation.

REFERENCES

Andersen RA, Essick GK, Siegel RM. Encoding of spatial location by posterior parietal neurons. *Science* 230: 456–458, 1985.

Batista AP, Buneo CA, Snyder LH, Andersen RA. Reach plans in eye-centered coordinates. *Science* 285: 257–260, 1999.

Batista AP, Santhanam G, Yu BM, Ryu SI, Afshar A, Shenoy KV. Heterogeneous coordinate frames for reaching in macaque PMd. *Soc Neurosci Abstr* 363.312, 2005.

Batista AP, Santhanam G, Yu BM, Ryu SI, Shenoy KV. Coordinate frames for reaching in macaque dorsal premotor cortex (PMd). *Soc Neurosci Abstr* 191.197, 2004.

Batista AP, Yu BM, Santhanam G, Ryu SI, Afshar A, Shenoy K. Cortical neural prosthesis performance improves when eye position is monitored. *IEEE Trans Neural Syst Rehab Eng* In press.

Boussaoud D. Primate premotor cortex: modulation of preparatory neuronal activity by gaze angle. *J Neurophysiol* 73: 886–890, 1995.

Boussaoud D, Bremmer F. Gaze effects in the cerebral cortex: reference frames for space coding and action. *Exp Brain Res* 128: 170–180, 1999.

Boussaoud D, Jouffrais C, Bremmer F. Eye position effects on the neuronal activity of dorsal premotor cortex in the macaque monkey. *J Neurophysiol* 80: 1132–1150, 1998.

Bradley DC, Maxwell M, Andersen RA, Banks MS, Shenoy KV. Mechanisms of heading perception in primate visual cortex. *Science* 273: 1544–1547, 1996.

Buneo CA, Jarvis MR, Batista AP, Andersen RA. Direct visuomotor transformations for reaching. *Nature* 416: 632–636, 2002.

Caminiti R, Ferraina S, Johnson PB. The sources of visual information to the primate frontal lobe: a novel role for the superior parietal lobule. *Cereb Cortex* 6: 319–328, 1996.

Caminiti R, Johnson PB, Galli C, Ferraina S, Burnod Y. Making arm movements within different parts of space: the premotor and motor cortical representation of a coordinate system for reaching to visual targets. *J Neurosci* 11: 1182–1197, 1991.

Churchland MM, Afshar A, Shenoy KV. A central source of movement variability. *Neuron* 52: 1085–1096, 2006a.

Churchland MM, Santhanam G, Shenoy KV. Preparatory activity in premotor and motor cortex reflects the speed of the upcoming reach. *J Neurophysiol* 96: 3130–3146, 2006b.

Churchland MM, Shenoy KV. Delay of movement caused by disruption of cortical preparatory activity. *J Neurophysiol* 97: 348–359, 2007.

Churchland MM, Yu BM, Ryu SI, Santhanam G, Shenoy KV. Neural variability in premotor cortex provides a signature of motor preparation. *J Neurosci* 26: 3697–3712, 2006c.

Cisek P, Kalaska JF. Modest gaze-related discharge modulation in monkey dorsal premotor cortex during a reaching task performed with free fixation. *J Neurophysiol* 88: 1064–1072, 2002.

Cohen YE, Andersen RA. Reaches to sounds encoded in an eye-centered reference frame. *Neuron* 27: 647–652, 2000.

Deneve S, Duhamel JR, Pouget A. Optimal sensorimotor integration in recurrent cortical networks: a neural implementation of Kalman filters. *J Neurosci* 27: 5744–5756, 2007.

Deneve S, Latham PE, Pouget A. Efficient computation and cue integration with noisy population codes. *Nat Neurosci* 4: 826–831, 2001.

Duhamel JR, Bremmer F, BenHamed S, Graf W. Spatial invariance of visual receptive fields in parietal cortex neurons. *Nature* 389: 845–848, 1997.

Dum RP, Strick PL. The origin of corticospinal projections from the premotor areas in the frontal lobe. *J Neurosci* 11: 667–689, 1991.

Dum RP, Strick PL. Frontal lobe inputs to the digit representations of the motor areas on the lateral surface of the hemisphere. *J Neurosci* 25: 1375–1386, 2005.

Fu QG, Suarez JI, Ebner TJ. Neuronal specification of direction and distance during reaching movements in the superior precentral premotor area and primary motor cortex of monkeys. *J Neurophysiol* 70: 2097–2116, 1993.

Galea MP, Darian-Smith I. Multiple corticospinal neuron populations in the macaque monkey are specified by their unique cortical origins, spinal terminations, and connections. *Cereb Cortex* 4: 166–194, 1994.

Georgopoulos AP, Schwartz AB, Kettner RE. Neuronal population coding of movement direction. *Science* 233: 1416–1419, 1986.

Graziano MS, Gross CG. Visual responses with and without fixation: neurons in premotor cortex encode spatial locations independently of eye position. *Exp Brain Res* 118: 373–380, 1998.

Graziano MS, Hu XT, Gross CG. Coding the locations of objects in the dark. *Science* 277: 239–241, 1997a.

Graziano MS, Hu XT, Gross CG. Visuospatial properties of ventral premotor cortex. *J Neurophysiol* 77: 2268–2292, 1997b.

Graziano MS, Yap GS, Gross CG. Coding of visual space by premotor neurons. *Science* 266: 1054–1057, 1994.

He SQ, Dum RP, Strick PL. Topographic organization of corticospinal projections from the frontal lobe: motor areas on the lateral surface of the hemisphere. *J Neurosci* 13: 952–980, 1993.

Jackson A, Mavoori J, Fetz EE. Long-term motor cortex plasticity induced by an electronic neural implant. *Nature* 444: 56–60, 2006.

Kakei S, Hoffman DS, Strick PL. Muscle and movement representations in the primary motor cortex. *Science* 285: 2136–2139, 1999.

Kalaska JF, Cohen DA, Hyde ML, Prud'homme M. A comparison of movement direction-related versus load direction-related activity in primate motor cortex, using a two-dimensional reaching task. *J Neurosci* 9: 2080–2102, 1989.

Kalaska JF, Scott SH, Cisek P, Sergio LE. Cortical control of reaching movements. *Curr Opin Neurobiol* 7: 849–859, 1997.

Kelly RC, Smith MA, Samonds JM, Kohn A, Bonds AB, Movshon JA, Lee TS. Comparison of recordings from microelectrode arrays and single electrodes in the visual cortex. *J Neurosci* 27: 261–264, 2007.

Kurata K, Hoffman DS. Differential effects of muscimol microinjection into dorsal and ventral aspects of the premotor cortex of monkeys. *J Neurophysiol* 71: 1151–1164, 1994.

Lu MT, Preston JB, Strick PL. Interconnections between the prefrontal cortex and the premotor areas in the frontal lobe. *J Comp Neurol* 341: 375–392, 1994.

Matelli M, Govoni P, Galletti C, Kutz DF, Luppino G. Superior area 6 afferents from the superior parietal lobule in the macaque monkey. *J Comp Neurol* 402: 327–352, 1998.

Matsumura M, Kubota K. Cortical projection to hand-arm motor area from post-arcuate area in macaque monkeys: a histological study of retrograde transport of horseradish peroxidase. *Neurosci Lett* 11: 241–246, 1979.

Messier J, Kalaska JF. Covariation of primate dorsal premotor cell activity with direction and amplitude during a memorized-delay reaching task. *J Neurophysiol* 84: 152–165, 2000.

Moll L, Kuypers HG. Premotor cortical ablations in monkeys: contralateral changes in visually guided reaching behavior. *Science* 198: 317–319, 1977.

Pesaran B, Nelson MJ, Andersen RA. Dorsal premotor neurons encode the relative position of the hand, eye, and goal during reach planning. *Neuron* 51: 125–134, 2006.

Picard N, Strick PL. Imaging the premotor areas. *Curr Opin Neurobiol* 11: 663–672, 2001.

Pouget A, Deneve S, Duhamel JR. A computational perspective on the neural basis of multisensory spatial representations. *Nat Rev* 3: 741–747, 2002.

Pouget A, Snyder LH. Computational approaches to sensorimotor transformations. *Nat Neurosci* 3, *Suppl*: 1192–1198, 2000.

Riehle A, Requin J. The predictive value for performance speed of preparatory changes in neuronal activity of the monkey motor and premotor cortex. *Behav Brain Res* 53: 35–49, 1993.

Sahani M. *Latent Variable Models for Neural Data Analysis* (PhD thesis). Computation and Neural Systems Program. Pasadena, CA: California Institute of Technology, 1999.

Santhanam G, Linderman MD, Gilja V, Afshar A, Ryu SI, Meng TH, KV S. HermesB: A continuous neural recording system for freely behaving primates. *IEEE Trans Biomed Eng* In press.

Santhanam G, Ryu SI, Yu BM, Afshar A, Shenoy KV. A high-performance brain-computer interface. *Nature* 442: 195–198, 2006.

Santhanam G, Sahani M, Ryu SI, Shenoy KV. An extensible infrastructure for fully automated spike sorting during online experiments. In: *Proceedings of the 26th Annual International Conference of the IEEE EMBS.* San Francisco, CA: *IEEE Eng Med Biol Soc*, 2004, p. 4380–4384.

Scott SH, Kalaska JF. Reaching movements with similar hand paths but different arm orientations. I. Activity of individual cells in motor cortex. *J Neurophysiol* 77: 826–852, 1997.

Scott SH, Sergio LE, Kalaska JF. Reaching movements with similar hand paths but different arm orientations. II. Activity of individual cells in dorsal premotor cortex and parietal area 5. *J Neurophysiol* 78: 2413–2426, 1997.

Shenoy KV, Bradley DC, Andersen RA. Influence of gaze rotation on the visual response of primate MSTd neurons. *J Neurophysiol* 81: 2764–2786, 1999.

Snyder LH, Grieve KL, Brotchie P, Andersen RA. Separate body- and world-referenced representations of visual space in parietal cortex. *Nature* 394: 887–891, 1998.

Sober SJ, Sabes PN. Flexible strategies for sensory integration during motor planning. *Nat Neurosci* 8: 490–497, 2005.

Stricanne B, Andersen RA, Mazzoni P. Eye-centered, head-centered, and intermediate coding of remembered sound locations in area LIP. *J Neurophysiol* 76: 2071–2076, 1996.

Tanne-Gariepy J, Rouiller EM, Boussaoud D. Parietal inputs to dorsal versus ventral premotor areas in the macaque monkey: evidence for largely segregated visuomotor pathways. *Exp Brain Res* 145: 91–103, 2002.

Weinrich M, Wise SP. The premotor cortex of the monkey. *J Neurosci* 2: 1329–1345, 1982.

Wu W, Hatsopoulos NG. Coordinate system representation of movement direction in the premotor cortex. *Exp Brain Res* 176: 652–657, 2007.

Yu BM, Kemere C, Santhanam G, Afshar A, Ryu SI, Meng TH, Sahani M, Shenoy KV. Mixture of trajectory models for neural decoding of goal-directed movements. *J Neurophysiol* 97: 3763–3780, 2007.

Zipser D, Andersen RA. A back-propagation programmed network that simulates response properties of a subset of posterior parietal neurons. *Nature* 331: 679–684, 1988.